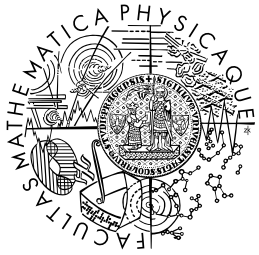

FACULTY
OF MATHEMATICS
AND PHYSICS
Charles University

Bachelor thesis

Juraj Májek

Fractal growth of polyethylene nanoislands on polyethylene oxide thin films

Department of Macromolecular Physics

Supervisor of the bachelor thesis: RNDr. Artem Ryabov, Ph.D.

Study programme: Physics

Study branch: General Physics

Prague 2019

I declare that I carried out this bachelor thesis independently, and only with the cited sources, literature and other professional sources.

I understand that my work relates to the rights and obligations under the Act No. 121/2000 Sb., the Copyright Act, as amended, in particular the fact that the Charles University has the right to conclude a license agreement on the use of this work as a school work pursuant to Section 60 subsection 1 of the Copyright Act.

In Prague date ..... Juraj Májek

I would like to thank my wonderful supervisor, RNDr. Artem Ryabov, Ph.D., for all his patient guidance, for all the advice he has given me and for the joys of discovery we have shared. Thank you for being someone I can look up to in many ways. I am truly grateful for working with you.

I would also like to express gratitude to the many excellent teachers I have been gifted with during my education.Thank you for doing your work with passion, even though you rarely receive the credit you deserve. It is invaluable.

A big thanks also goes to everyone who has shared both the better and the worse moments of life with me, to all my friends and to my beloved girlfriend, Anežka. Thank you for being here with me and for me.

I would like to dedicate this thesis to my family: to my father, to my mother, to my brother, Mišo, and to my aunts, Eva and Zuzana. Thank you for everything, mainly for all the love you have given me. Each one of you nurtured me in a special, distinct way and without it, a part of who I am today would be missing. Thank you.

Title: Fractal growth of polyethylene nanoislands on polyethylene oxide thin films

Author: Juraj Májek

Department: Department of Macromolecular Physics

Supervisor: RNDr. Artem Ryabov, Ph.D., KMF MFF UK

Abstract: Plasma polymer fragments deposited from vapor on non-wetting polymer substrates are seen to aggregate into fractal nanoislands. Dependent on conditions of the experiment, the islands attain diverse shapes ranging from dendritic snowflakes, branching seaweed to twisting snakes. In our work, we identify dominant kinetic processes responsible for this diversity and relate them to physical characteristics of the experiment [1].

We review and implement basic computer models of deposition and aggregation of diffusing particles: The Diffusion-Limited Aggregation (DLA) [2], both on a lattice and without a lattice, and the Cluster-Cluster Aggregation (CCA) [3]. The off-lattice DLA yields isotropic random fractals. The lattice DLA fractals are influenced by the properties of the lattice itself, which can be chosen to represent the symmetry of the substrate layer on which the islands grow. Fractals generated in the CCA model are more linear. Competition between diffusion and deposition rates gives a transition between off-lattice DLA and CCA fractals.

Each of these models comprises a mechanism that we conjecture to be dominant during growth of distinct observed polyethylene nanoislands. Thus the multiple observed fractal shapes allow us to draw conclusions on microscopic kinetics of the surface diffusion of deposited polymer fragments. The gained insight into the kinetics may be relevant for plasma-assisted development of polymer-based devices.

Keywords: Plasma polymers, Fractal growth, Diffusion-limited aggregation, Cluster-cluster aggregation

Contents

Introduction

This thesis is an effort to theoretically model fractal patterns observed in an experiment in Ref. [1]. The goal of the thesis is to explain changes of patterns grown on a thin polymer film in a certain setting. On the film grow islands (also called clusters) shaped like on Fig. 1a or 1b. The difference between the two patterns is tremendous, but the changes in experimental conditions only slight. In this work we develop a model that can describe such diverse patterns. Understanding the mechanisms of growth will allow for deeper insight into the processes in polymer coated surfaces.

In this chapter, we will introduce the basic theoretical framework for analysis of fractals and the basics of the experiment this work deals with.

Plasma Polymers

Conventional polymers are formed by repeating of the same units in a long chain or network. Though their chemical structure is organized, the overall shape of the molecules is random. Long macromolecular chains curl into random coils, which can be stretched easily, thus giving name to the field of soft matter [4].

Plasma polymers are created by applying plasma to a precursor, which can be a monomer or a conventional polymer. The plasma fragments the precursor molecules. The sites of fragmentation become reactive radicals, which then bind to other molecules.

The chemical structure of molecules formed this way is disordered and often different from that of the precursors, an example is on Fig. 2. Plasma polymers can have unsaturated bonds, even if their precursor did not. They are typically highly cross-linked, which makes them more rigid.

A useful application of these polymers is that they can easily be grown on a surface and act as a coating. This is achieved simply by placing the coated surface near the plasma where fragments are generated. This allows for development of diverse polymeric thin films. One of such is modelled in this work, where polyethylene (PE) was deposited on polyethylene oxide (PEO) coated surface.

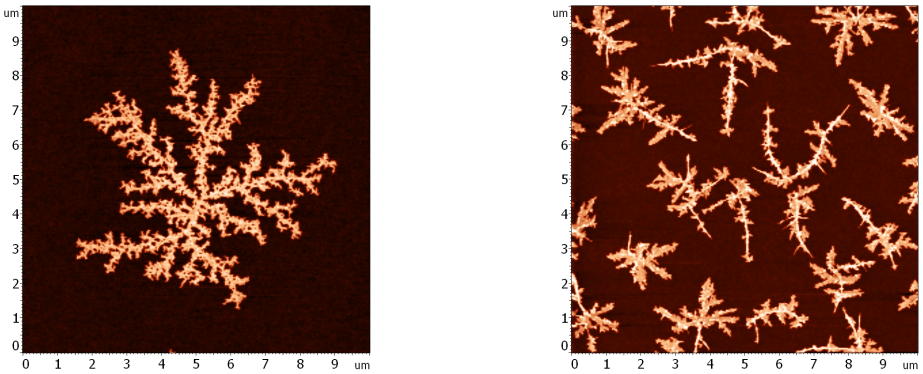

(a) A randomly branched isotropic fractal (b) Linear anisotropic fractals

Figure 1: AFM images of polyethylene islands grown on polyethylene oxide thin films prepared in Ref. [1].

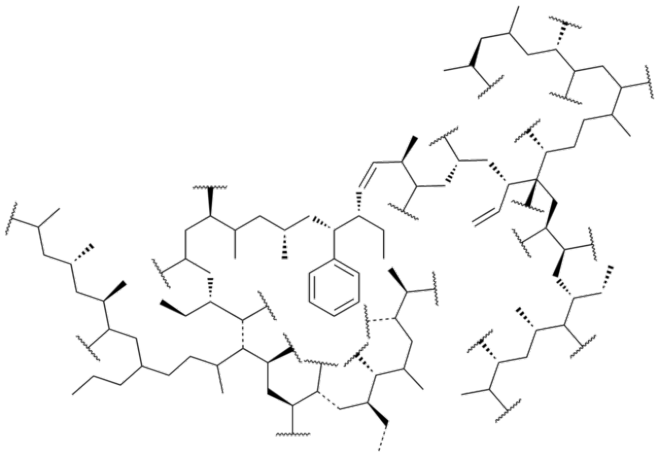

Figure 2: A hypothetical structure of plasma-polymerized ethylene film, taken from Wikimedia Commons [5].

Fractal Growth

Fractals were first conceived as purely mathematical objects. Their basic characteristic is that they consist of repeating patterns on all length scales. For mathematical fractals, this is ensured by defining the object recursively: the shape of the fractal on one scale is deterministically governed by its shape on another scale.

Fractals also grow in many real-life settings, both in nature and society. These patterns are almost always not deterministic [6]. Their growth is random and there are no explicit recursive rules making the object self-similar. The self-similarity arises spontaneously, usually thanks to the object substructures competing with each other. In most cases, the competition is to ensure effective filling of space. This is the case for growth of city streets or branched organs, such as lungs or kidneys.

New streets in a city grow where there are no existing ones to cover the area. They connect this new area to an existing street, which then becomes more important. This way the set of streets acquires self-similar hierarchy, as from important streets grow less important ones. This hierarchy ensures effective transport of resources from the higher, global scales into the local ones [7].

A recent theory of growth of branched organs in Ref. [8] states three rules to which the growing organ tips adhere:

1. The tip can elongate itself in a random direction
2. The tip can branch into two new ones, which grow independently
3. When the tip gets too close to another branch, its growth terminates (the branches send out signal molecules which ensure this)

These rules give rise to the fractal morphology of lungs. As branches growing in proximity inhibit each other, only those branches which grow in unfilled areas grow long. This mechanism again ensures effective space-filling.

Space filling is also at work for polymer nanoislands. It will be shown later in the thesis that the shape of the cluster grown in Fig. 1 also arises from the competition for space.

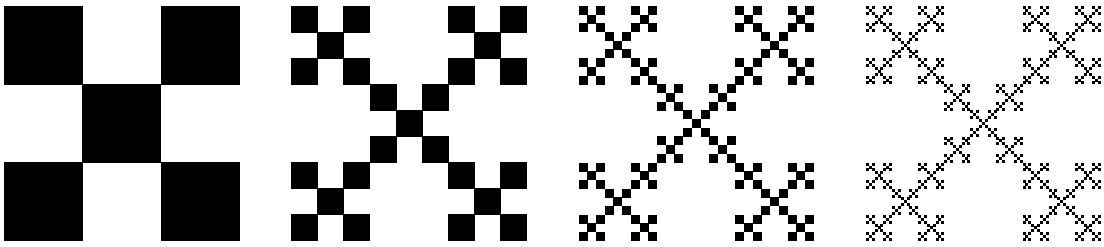

Figure 3: The Vicsek fractal with $\mathcal{D} = \frac{\log 5}{\log 3}$, taken from Wikimedia Commons [10].

Fractal Dimension

The basic measure used to define fractals and describe them quantitatively is the *fractal dimension* $\mathcal{D}$ [9]. Many equivalent definitions exist, but here we will use one natural for growing fractals:

Suppose an object (of any shape, not necessarily a self-similar one) is built from elementary particles of length 1. If the object is to have length 1, it will naturally consist of one particle. If it is to have length 2, it depends. For a square, one would need four particles, for a cube, eight. The number of needed particles N scales with the second power of length L for squares, which are two-dimensional and with exponent 3 for three-dimensional cubes. This exponent defined as the fractal dimension $\mathcal{D}$ of the object. In equation form:

$$N \sim L^{\mathcal{D}} \tag{1}$$

Fractals are then defined as object with non-integer fractal dimension. The Vicsek fractal in Fig. 3, for example, has $\mathcal{D} = \frac{\log 5}{\log 3}$, as for every tripling of size, five times more particles are needed to build it.

In the following two chapters we discuss two basic models describing fractal growth. These models assume that particles merging into the fractal island diffuse freely on the surface. The model in Chap. 1 creates patterns similar to Fig. 1a, the model in Chap. 2 patterns similar to Fig. 1b. A more detailed analysis of the latter model is presented in Appendix A. Chap. 3 unifies these two models into a more robust one, which allows the explanation of morphology changes proposed in Chap. 4.

1. Diffusion-Limited Aggregation

Diffusion-limited aggregation (DLA) developed in Ref. [2] is the first and simplest among the fractal growth models based on irreversible aggregation of diffusing particles.

In DLA, only one cluster grows at a time, starting from a static seed particle located at the origin of coordinates. In every step of the simulation a new particle is placed at a random position far from the seed. Then it undergoes a random walk until it hits the cluster. After hitting, the particle becomes a part of the cluster, and a new simulation step begins.

Islands grown by this model have typically the shape of a randomly branched fractal. What creates these patterns are not the branches themselves, but the spaces between them ('fjords') [11]. When some part of the growing island lags behind its neighbors, it becomes encroached by two branches. These shield it from the diffusing particles and it grows even slower.

The DLA-like fractals occur in nature in rather diverse and seemingly unrelated settings [12]. Most prominent example include aggregation of dust particles [2] and growth of fractals in solutions of electrolytes, for example in Ref [13]. In these cases the fractal actually grows by absorbing diffusing particles that come near to it. However, DLA can also describe processes such as viscous fingering (injection of a liquid into a more viscous one) or dielectic breakdown in an insulator [11].

All these phenomena are examples of Laplacian growth [12], which means the growth of the pattern is governed by a scalar field ϕ satisfying $\Delta\phi = 0$ with fixed constant ϕ at the cluster boundary. The growth speed of a place at cluster boundary is then proportional to $\nabla\phi$. The field ϕ can have many physical interpretations: electric potential in the case of dielectric breakdown, probability of location of a diffusing particle or pressure in the case of viscous fingering.

1.1 Lattice DLA

The fastest way to simulate the DLA is to consider the particle motion on a discrete square lattice, so each particle occupies one lattice site. At each movement step the particle chooses one of the four directions randomly. When it comes to a site adjacent (sidewise or diagonally) to the cluster, it becomes fixed at that site as a part of the island.

In [11] the fluctuations were damped by introducing an integer parameter s describing the stickiness of the cluster. Particles still diffuse until they reach the fractal, but now a lattice site is added to the cluster only after s particles have hit it at that site. This takes a small average over the fluctuating particle trajectories and so makes the cluster grow in a more ordered manner.

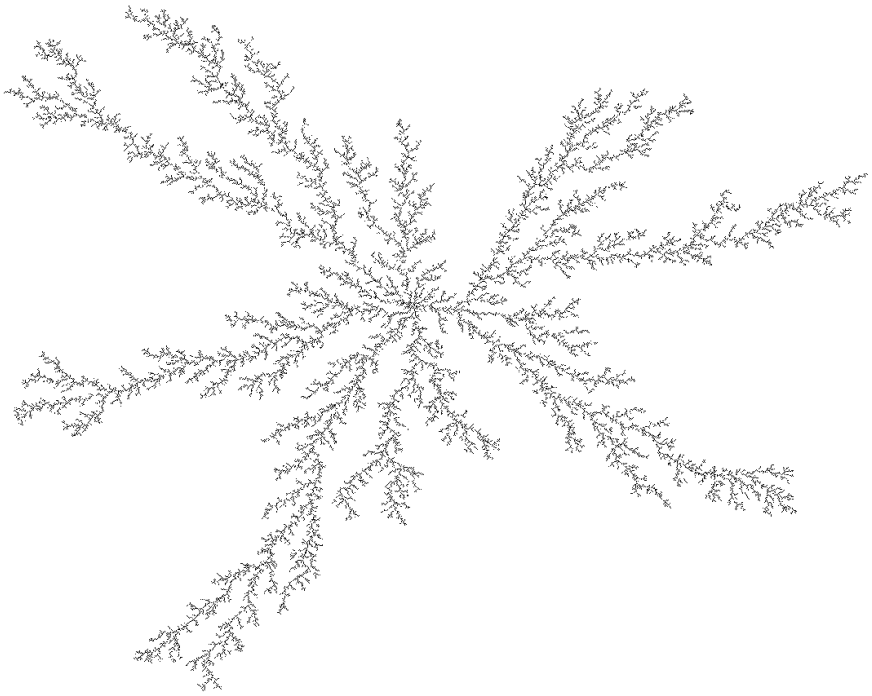

Figure 1.1: A DLA cluster with 40000 particles grown on a square lattice. It shows no preferred direction of growth and consists of branches encroaching fjords.

1.1.1 Implemented Algorithm

We have reproduced the algorithm proposed in Ref. [2] and simulated the model in *Octave* as follows:

The surface is represented as a square matrix of size L much larger than fully grown cluster size. The initial particle positions were chosen randomly in distance greater than current cluster radius. For every unoccupied lattice site, the number of particles that hit the cluster there is stored. When it reaches s, the site becomes occupied.

If the particle would move outside the grid, it is terminated instead. Also finite particle lifetime τ is implemented to speed up the simulation, which means that after τ steps the particle is also terminated. This was to cut off trajectories that were unreasonably slow to reach the cluster (moved in circles for example). τ was chosen large enough ($\tau \approx 3L$), so that almost all particles did not run out of steps. In reality, the diffusing polymer fragments could diffuse infinitely long, but since most particles in the simulation were unaffected by τ, this feature does not affect the resulting shape.

1.1.2 Results

Clusters with n_c (the number of particles in the cluster) up to 10^6 have been obtained. For $s = 1$, the fractals are visually same as in Ref. [2] (Fig. 1.1).

Results for higher s (Fig. 1.3 and 1.2) show that the branches grow preferentially in the diagonal direction of the lattice. This is because lattice sites the cluster neighbors diagonally are more easily accessed. Sites neighboring sidewise

are shielded by those neighboring diagonally. This creates an effective anisotropy in the lattice, which is more pronounced for higher s.

In Fig. 1.5, s was chosen smaller in the sidewise directions, so it would counteract the anisotropy of the lattice. The fractal follows the four sidewise directions, but secondary branches are again diagonal.

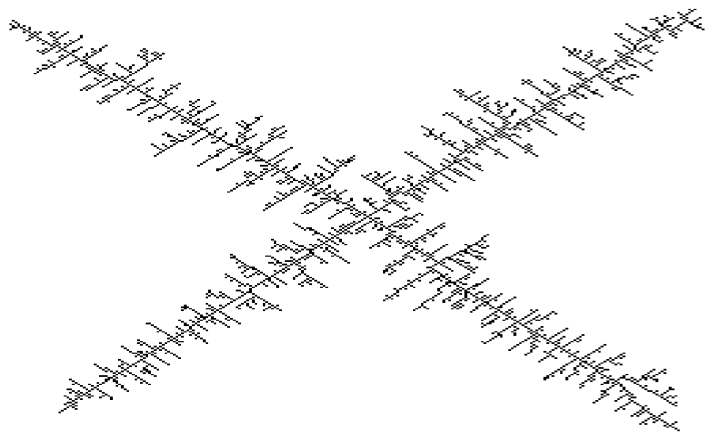

Figure 1.2: A lattice DLA fractal with $n_c = 3000$ grown with $s = 6$, showing amplified growth in diagonal directions.

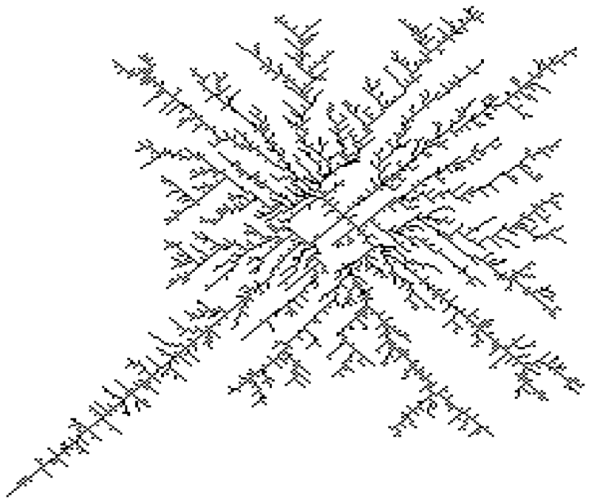

Figure 1.3: A lattice DLA fractal with $s = 2$ on the main lattice diagonal $s = 4$ elsewhere. The preference of diagonals is now weaker, though s is lower on them.

To summarize, results of the simulations are in accordance with Ref. [14]. It states that the resultant shape of the lattice DLA cluster is given by interplay of lattice anisotropy (in the case of a square lattice, the preference of diagonals) and random fluctuations brought in by diffusion. The fluctuations are damped either by increasing s or with growing cluster size, as the small differences brought

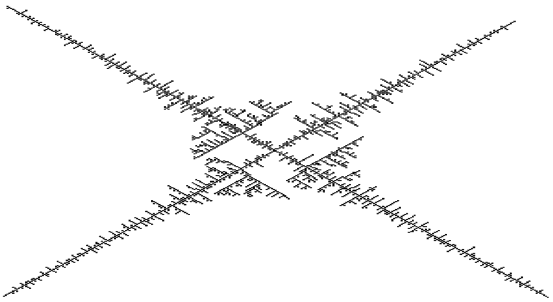

Figure 1.4: A lattice DLA fractal with $s = 10$ and $s = 5$ on the main lattice diagonal. The cluster attains a needle-like shape, as diagonals are greatly preferred.

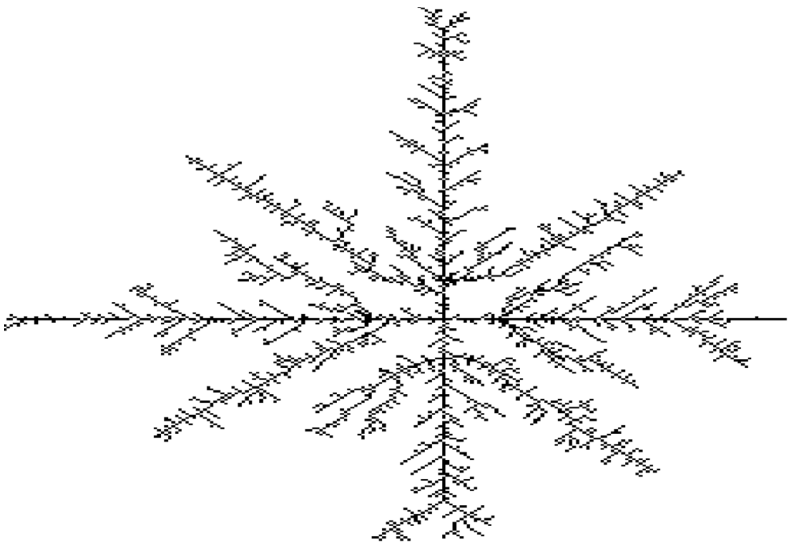

Figure 1.5: A lattice DLA fractal with $s = 1$ in the middle lattice column and row, $s = 6$ elsewhere. The anisotropic s fights with the anisotropy of the lattice.

about by anisotropy build up over time. The growth can be divided into three stages:

1. At first the cluster retains the typical DLA shape with circular envelope, as growth is dominated by fluctuations. The fractal dimension is $\mathcal{D} \approx 1.71$.

2. With increasing size the anisotropy becomes more important and branches in diagonal directions are preffered, creating a dendritic shape as in Fig 1.2.

3. Lastly the preference of the diagonals becomes so pronounced that the cluster grows almost entirely along them and forms a needle-like shape as in Fig. 1.4. $\mathcal{D} \to 1$.

Increasing s merely makes these transitions happen at lower n_c. For regular DLA ($s = 1$) only the first stage was retrieved (Fig. 1.1), for homogenous s the first two (Fig. 1.2) and for inhomogenous s all three.

In lattice DLA therefore the major factor determining the morphology of large clusters is the lattice itself. Different lattices produce different symmetries, for example in [11], a triangular lattice was chosen, and the resultant fractals had hexagonal symmetry thus resembling snowflakes.

In the modeled experiment the lattice can either represent the PEO layer or the Si substrate. PEO, a plasma polymer, was above its glass transition temperature in during deposition of PE. That means it was in an amorphous state and did not have any symmetric properties. To avoid bias from the lattice, a model without any lattice effects was investigated.

1.2 Off-lattice DLA

The lattice in DLA was originally implemented to ease the demands for memory and speed up the simulation, but as the lattice properties have major effect on the growth, a model working without any lattice was developed in Ref. [15].

In the off-lattice DLA, the particles have their own shape and aggregate when they intersect with a particle already in the cluster. As there is no lattice, they move according to overdamped Brownian motion [16] with diffusion constant D, where at every time step the displacement is proportional to a random normal variable $\vec{\xi}$.

1.2.1 Implemented Algorithm

The particle was initiated in a random position within a large circle of size L, if it would move outside it is terminated. With each movement step a random normal variable $\vec{\xi}$ was generated and the particle's position is updated according to:

$$\vec{r}(t + \mathrm{d}t) = \vec{r}(t) + \sqrt{D\mathrm{d}t}\ \vec{\xi}(t). \tag{1.1}$$

Also, the radius of the growing island l (largest distance from cluster seed) is computed after each aggregation. To avoid unnecessary diffusion steps, if the initial distance of the particle from the cluster seed was greater than l, it was transported straight towards the seed so that the distance equaled l. Because of this, lifetime had to be chosen infinite.

1.2.2 Results

The simulation was carried out with circular particles. In this case no transition to dendrites or needles was observed, and introducing stickiness s (only every sth particle that hit a certain particle of the cluster stuck to it) had no effect on fractal morphology, as there was no anisotropy in the model to amplify.

We have tried whether using anisotropic particles (for example, triangles oriented the same way) would change cluster morphology. On short distances (3-4 particles apart), the branches had a distinct orientation. However, the particles did not aggregate exactly in a given place (as was the case with lattice DLA), so on larger scales this was smeared out. The resulting clusters looked alike to those grown with circular particles.

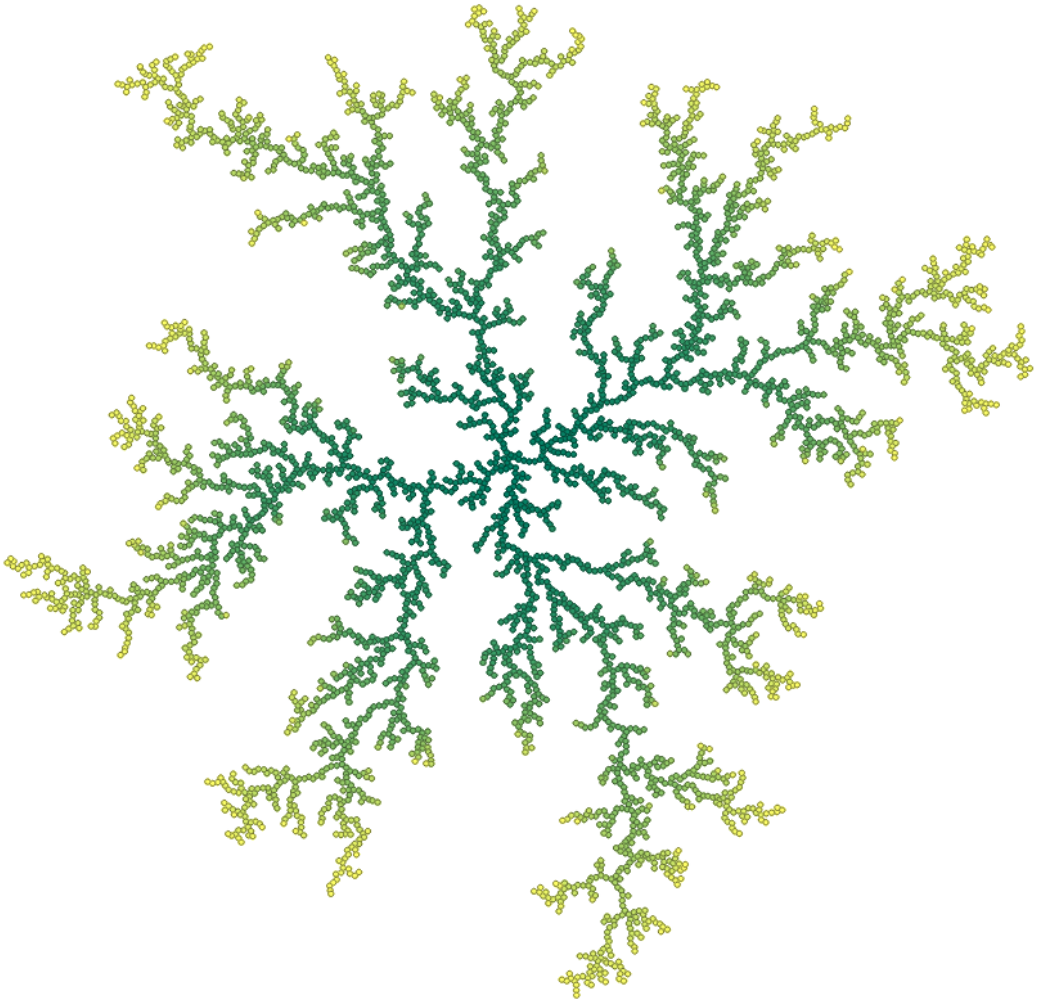

Figure 1.6: An off-lattice DLA fractal, $n_c = 4500$, color based on agregation order.

2. Cluster-Cluster Aggregation

Ordinary DLA models do not take into account many-body kinetic effects, namely the fact that other particles do not wait for the first to hit the cluster. They diffuse simultaneously and can hit each other. The cluster, too, can move, though slowly. To describe cluster growth in real time, *cluster-cluster aggregation* (CCA) was developed independently by Meakin [3] and Jullien [17].

In its simplest version, n particles (circular with radius a) are initiated randomly on the surface and simultaneously perform Brownian motion. If two particles hit each other, they stick and diffuse together. Typical clusters generated by this basic model are shown in Fig. 2.1. More realistic models include dependence of diffusion constant on cluster size.

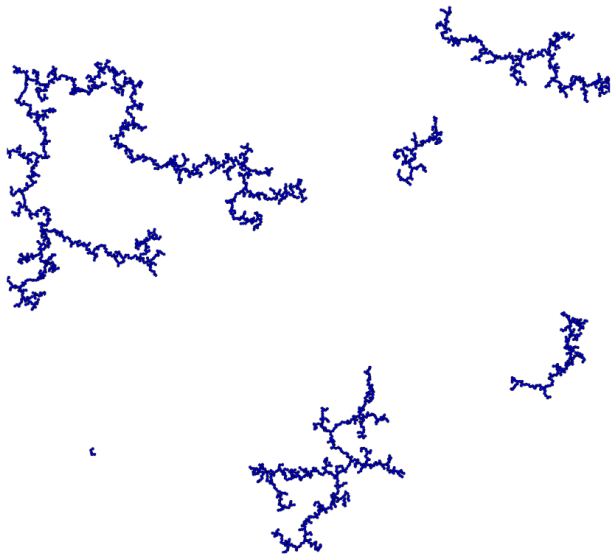

Figure 2.1: Typical clusters grown by CCA showing a degree of anisotropy and more linear morphology than in DLA, cf Fig. 1.6

2.1 Cluster Anisotropy

What is remarkable in this model is that the resulting fractals do not have circular envelopes or a distinct center. The model generates anisotropic shapes, without implementing any anisotropy into the growth rules. This symmetry breaking is generated simply by large amplifying of fluctuations.

In 2D, as written in Ref. [18], two merging clusters do not penetrate much on average. Therefore their contact happens close to their perimeter. Because of this, clusters with close-to-circular envelopes merge to form an anisotropic, 'stringy', cluster with length two times the width. On the other hand, too stringy clusters can overlap and so get more compact. This creates an equilibrium resulting in fractal dimension of $\mathcal{D} = 1.42$. The anisotropy can be characterized by the *anisotropy ratio* A, defined as the greater eigenvalue of the cluster inertia tensor divided by the lesser eigenvalue. For this model, we have $A = 5.7$ [19].

2.2 Low Concentration Limit

The low-density limit of this model is well understood and can be simulated easily as in Ref. [20]. Without actually simulating the whole process in real time, one can instead pick two clusters (based on rules described below), rotate them randomly, set them close to each other and let them move until they hit each other.

Growth in this limit can also be described using a system of coupled rate equations, one for every possible cluster size s. These are called the *Smoluchowski coagulation equations* [21], [22]:

$$\frac{\partial N(n_c,t)}{\partial t} = \frac{1}{2}\sum_{j=1}^{n_c-1} K(n_c-j,j)N(n_c-j,t)n(j,t) - \sum_{j=1}^{\infty} K(n_c,j)N(n_c,t)N(j,t) \tag{2.1}$$

where $N(n_c,t)$ is the number of clusters of size n_c at time t. $K(x,y)$ is called the reaction kernel, or reaction rate constant for the aggregation of clusters of size x and y. Here $K(x,y)$ depends on x and y for two reasons: because for larger clusters it is easier to hit each other; and because larger clusters move more slowly. The exact form from Ref. [23], assuming low concentration and a mean field approximation, is (the $1/\mathcal{D}$ dependence is from growing size and the $-1/\mathcal{D}$ is given by slower diffusion):

$$K(x,y) = \frac{x^{1/\mathcal{D}} + y^{1/\mathcal{D}}}{x^{-1/\mathcal{D}} + y^{-1/\mathcal{D}}}. \tag{2.2}$$

The simulation should be consistent with this reaction kernel. When choosing the two clusters (with sizes x and y) to react, one generates a random number ξ uniformly from $(0,1)$, and then, if $\xi > K(x,y)/K_{max}$, where K_{max} is the maximum value among $K(x,y)$, then the clusters are set to react. If $\xi < K(x,y)/K_{max}$, no aggregation happens. This way it is ensured that the clusters of different sizes actually react according to $K(x,y)$. However, in Ref. [20] it is stated that the resulting fractal dimension of the clusters does not depend much on the form of the reaction kernel, so also a constant one can also be used (then the aggregation happens always).

This limit is easier to simulate, but the AFM images of the islands from experiments in Chapter 4 clearly show that the clusters grow near each other. Thus, this simplified version could not be used and growth at finite concentrations was investigated instead, with algorithm explained on the following page.

2.3 Finite Concentration

For higher densities, the mean field approach applicable for dilute layers is not valid. The shapes of neighboring clusters are now not independent. Before neighboring islandS join, they grow in a complementary manner: where one island has an outward-pointing branch, the second will have an inward-pointing fjord, so the clusters will interlock each other as in Fig. 2.2. Because of this the interpenetration of the clusters is greater, which increases the fractal dimension. The magnitude of this effect, and also the resulting $\mathcal{D}$ depends on concentration.

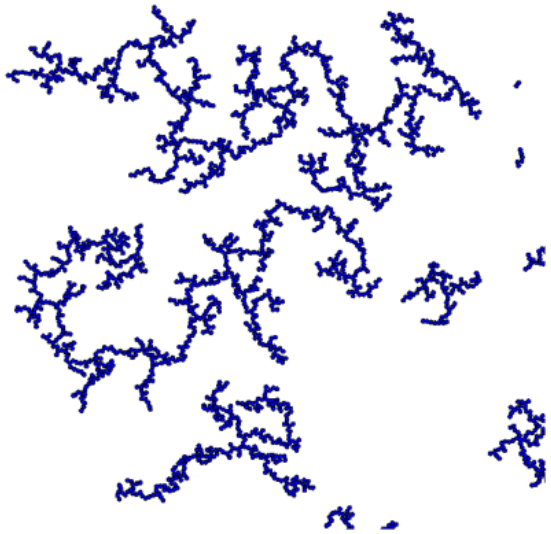

Figure 2.2: Interlocking of CCA clusters at high densities.

2.4 Implemented Algorithm

The CCA model was implemented in *Matlab*, both without an with scaling of diffusion constant D with cluster size n_c. The simulation algorithm is as follows:
Data structure: To make use of *Matlab*'s optimization of vector operations, the particle positions $\vec{r}_i$ are stored in one matrix of size $2 \times n$. The information about which particles belong to which cluster is in a *cell array* where the i-th cell contains for each particle in the i-th cluster the row number in the r-matrix where its position is stored.
Diffusion: If no aggregation occured in the simulation step, time is incremented by one and cluster positions are updated. Periodic boundary conditions were also implemented, so the particles are confined to a box of size $L \times L$. The physical time interval between two time steps is Δt.

In the movement step, a normal-distributed random 2×1 vector $\vec{\xi}$ is generated for each cluster. Then the position of every particle in the cluster is updated by:

$$\vec{r}_i(t + \Delta t) = \vec{r}_i(t) + \sqrt{D(n_c)\Delta t}\ \vec{\xi}_i(t) \mod L. \tag{2.3}$$

Aggregation: Computing pairwise distances between all particles to check aggregation would be ineffective, instead the so called *cell list* strategy [24] was used:

1. At each simulation step, the box was divided into a grid of squares with size of $2a$, stored in a matrix.

2. For every particle of the i-th cluster, the grid squares which overlap with it are found (this yields 2×2 squares).

3. It is checked if the squares did contain particles of a previous cluster.

4. If yes, then the distance between the current particle and all particles of such cluster is computed and it is checked whether they aggregate.

5. If aggregation did not occur, then the grid squares are marked 'containing i-th clusterÂt, and the loop continues from step 2 for another particle from the same cluster. If all particles in the cluster are checked, then the first particle of the $i+1$-th cluster is chosen.

2.5 Results

The simulation resulted in typical stringy fractals known from Ref. [20] or [17], examples are shown in Fig. 2.4 and 2.3.

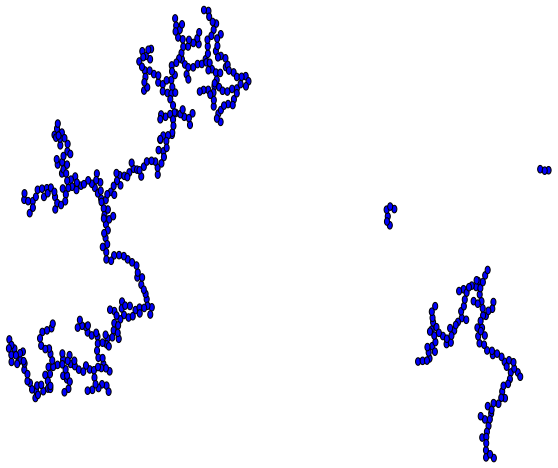

Figure 2.3: Two CCA fractals with $n_c = 369$ (left) and 98 (right).

The method for computing the fractal dimension $\mathcal{D}$ was as in Ref. [17]. The method uses radius of gyration R of the clusters to obtain $\mathcal{D}$. R can be easily calculated as the standard deviation of the cluster particle centers. The scaling of R with n_c is the same as that of L_c, or any other length characteristic of the growing fractal:

$$R \sim n_c^{\frac{1}{\mathcal{D}}} \tag{2.4}$$

The growth was simulated, and after each cluster collision, the n_c and R of the newborn cluster was calculated. From these $\mathcal{D}$ was obtained as the inverse slope of a linear fit of the dependence of $\log R$ on $\log n_c$ shown in Fig. 2.5.

The obtained value of $\mathcal{D} = 1.36$ is close to the value 1.42 obtained in [17], where the low concentration limit was simulated. The fluctuations of R for given n_c are results both of the random nature of the fractals and, of finite time step Δt of the simulation, thanks to which the clusters did not aggregate immediately at contact, but could overlap slightly. The first effect effect is dominant for larger n_c and the second for n_c smaller.

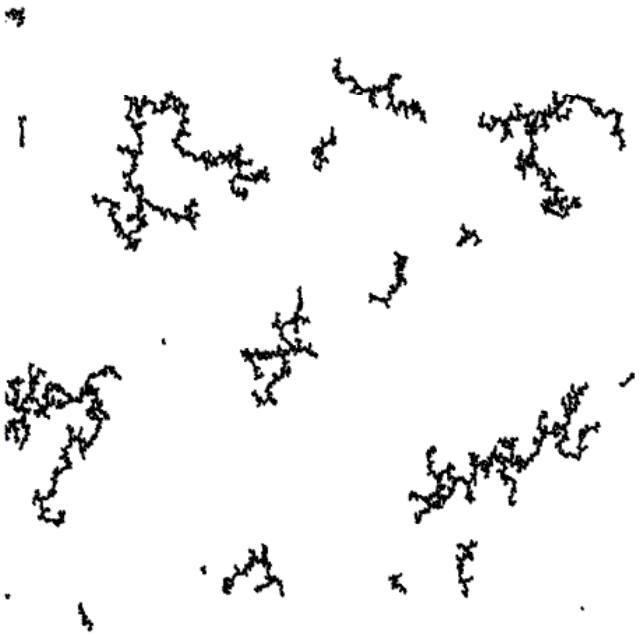

Figure 2.4: An illustration of typical large CCA clusters.

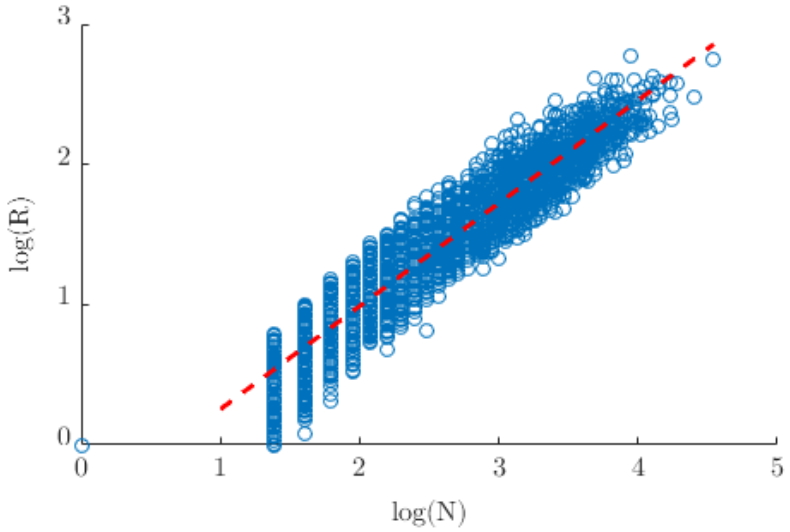

Figure 2.5: Logarithmic plot of R on n_c, results from 18000 clusters generated from simulation of 40000 monomers with density $d = 1.8 \cdot 10^{-2}$. $\mathcal{D} = 1.36$.

3. Deposition Diffusion Aggregation

In the experiment, particles are deposited onto the surface gradually. The simpler models, DLA and CCA dealt with deposition in an idealized way: in DLA it was infinitely slow, in CCA deposition happens only at the beginning. In this chapter an extended model is presented, that deals with deposition realistically. It encompasses both DLA and CCA. Thanks to this, it will allow us to see how changes of the experimental parameters determine which simpler model can describe the growth.

This generalization is called the DDA model (Deposition, Diffusion, Aggregation). In it, particles enter the surface with flux F (defined as the number of particles entering a unit area per unit of time).

The behaviour of the growing surface changes with growth and can be structured into the following stages [25]:

1. The surface is initiated almost empty with monomers far from each other. The number of monomers increases.

2. The monomers start to aggregate, forming oligomers. The numbers of monomers and olimogers both increase.

3. The oligomers are now widespread enough that they capture monomers faster than they arrive. The islands grow mostly by capturing monomers.

4. The islands are so large now that the number of monomers is negligible, new particles are caught almost immediately. The growth furthers mostly by joining of existing islands.

5. The islands slowly join each other, until they become part of a single cluster spanning the entire surface. This is called the *gelation point.*

3.1 Kinetic Phase Diagram

What is most remarkable about this model is that it can generate both stringy fractals shaped like those grown by CCA and also circular DLA-shaped islands. The resulting shape is given by competition between two timescales: that of diffusion of existing particles and deposition of new ones.

When diffusion is much faster than deposition, the model effectively reduces to off-lattice DLA, because, on average, when a new monomer appears, it hits an island before another monomer is deposited. This way the islands grow by capturing monomers, instead of oligomers, which is what creates the DLA shape. The joining of two islands happens rarely, as they diffuse slowly compared to monomers.

The number of islands simultaneously growing on the surface is also given by the ratio of the timescales. If deposition would be infinitely slow, all particles would aggregate into one island everytime between new particle arrivals, which

is precisely the DLA model. As deposition gets faster, more islands grow on their own, and the growth slowly changes into CCA.

The mechanism of the growth determines the shape of the gelation cluster. A phase diagram taken from [25] showing the shape transition boundaries for different F and system size L is in Fig 3.1. With growing F the gelation cluster shape changes from DLA to CCA to a percolation cluster, which grows when diffusion is negligible compared to deposition.

For gelation, the shape also depends on surface size L, as when L is large enough for many islands to grow on the surface, the resulting spanning cluster is always CCA-shaped, as it is generated by joining of the islands, which means that it does not have a center point like DLA fractals. The spanning cluster is DLA-shaped only if a single (or very few) island grows on the surface. In the described experiment, gelation was not reached on the acquired AFM images in Chap. 4. For systems before gelation the behaviour is independent on L and depends only on the ratio F/D.

The transition also depends on how diffusion constant scales with cluster size. In the diagram in Fig. 3.1 as well as in the simulations in this chapter, the scaling was assumed to be:

$$D(n_c) = D_0 n_c^{\gamma} \tag{3.1}$$

with $\gamma = -1$. The value of γ influeces positions of the phase boundaries in the diagram: with higher γ the transitions happen at lower F and the CCA phase slowly disappears. For $\gamma \to \infty$ only the DLA and percolation phases exist [25].

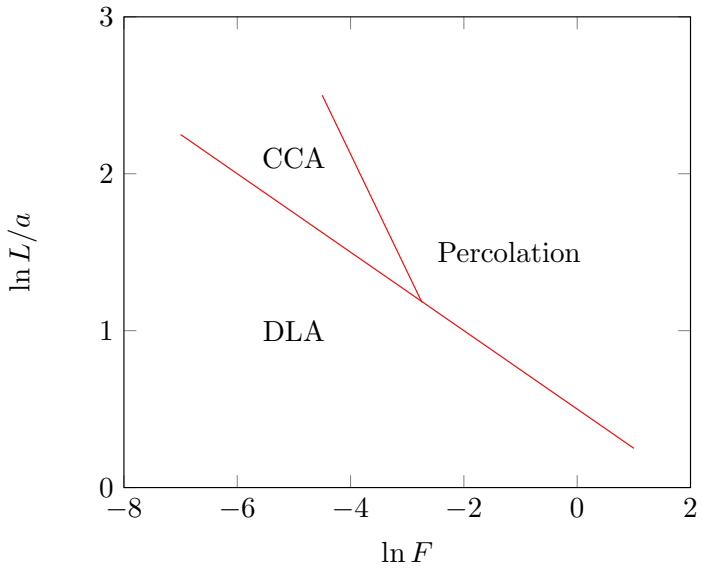

Figure 3.1: DDA morphology phase diagram reproduced from Ref. [25], showing the transitions between different spanning cluster shapes. The diagram is constructed for $D(n_c) \sim n_c^{-1}$.

3.2 Implemented Algorithm

The algorithm is the same as in Chap. 2, with the addition of one feature:
Deposition: *Deposition time* τ_d was introduced, so that every τ_d-th simulation step, a new monomer was added onto the surface with a random position. This yields a flux of

$$F = \frac{1}{\tau_d L^2} \tag{3.2}$$

For quicker simulation, the positions of all particles (not only the initial) were generated and stored in r at the beginning. Until the particle appeared at the surface, it was not moved or considered for aggregation.

The exact code is listed in Attachment B.

3.3 Results

We have simulated the DDA model for a range of F with constant D. For each simulation, we have captured the growth for different stages, given by different particle density defined as

$$d = n\frac{\pi a^2}{L^2}. \tag{3.3}$$

We have retrieved the three morphologies in Fig. 3.1, their growth is shown in Fig. 3.4, 3.5 and 3.6. Our results confirm the findings in Ref. [25]: for boosting F, the fractal shapes change from DLA to CCA to percolation.

However, a closer analysis indicates that the three regimes are actually not distinct phases. For a range of F and fixed D, we have computed $\mathcal{D}$ for given density and obtained values in Tab. 3.1. They are plotted in Fig. 3.2, and as can be seen, $\mathcal{D}$ changes continuously with F. It has no jumps as in a phase transition.

Each DDA regime is characterised by one dominant growth mechanism (diffusion of monomers for DLA, diffusion of clusters for CCA, deposition for percolation). However, every mechanism is still present also in the other regimes, it is only weaker. The relative strengths of these mechanisms change continuously with F. Therefore, also the regimes change into one another continuously.

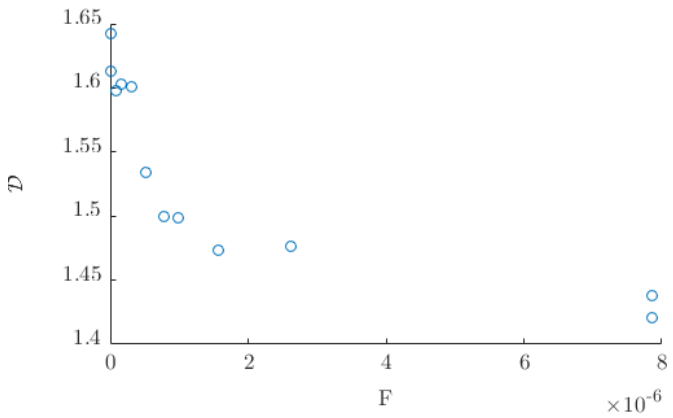

Figure 3.2: Plot of $\mathcal{D}$ as the function of F for $D(n_c) \sim n_c^{-1}$, showing the change of island morphology for different DDA regimes.

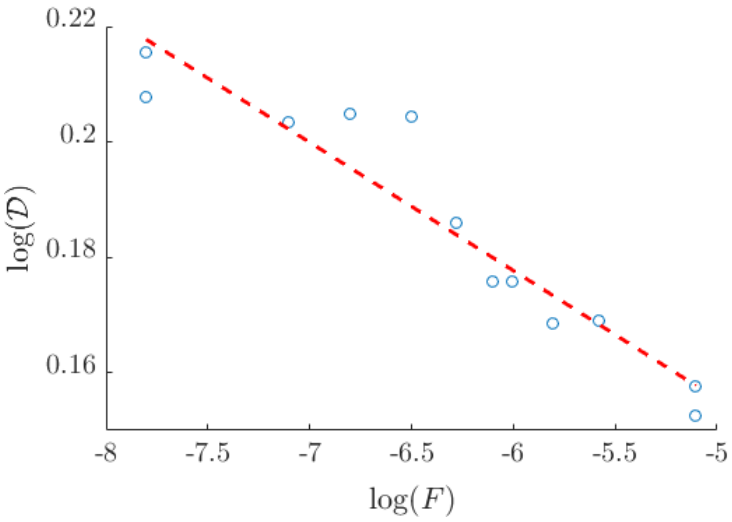

Figure 3.3: Logarithmic plot of $\mathcal{D}$ as the function of F for $D(n_c) \sim n_c^{-1}$, showing the change of island morphology for different DDA regimes. The dependence is fitted with $\mathcal{D} \sim F^{\kappa}$ with $\kappa \approx -0.2$.

$F \cdot 10^{-8}$	786.5	786.5	262.2	157.3	98.32	78.65
$\mathcal{D}$	1.437	1.421	1.476	1.474	1.499	1.499
$F \cdot 10^{-8}$	52.44	31.46	15.73	7.865	1.573	1.573
$\mathcal{D}$	1.534	1.601	1.603	1.598	1.613	1.642

Table 3.1: Fractal dimension $\mathcal{D}$ of DDA clusters grown for different F for $d = 0.1$. The clusters were grown with $a = 1$, $L = 200$, $D = 0.1$. $\mathcal{D}$ was calculated using the method from Chap. 2. Each value of $\mathcal{D}$ was computed from at least 100 clusters, except those for $F = 1.573 \cdot 10^{-8}$, for which 29 and 41 clusters were used.

For high F/D in Fig. 3.4, many small clusters are growing, and they seldom manage to merge. Diffusion is not important at all and the behaviour can be modelled as that of a percolation cluster.

For medium F/D in Fig. 3.5, larger islands grow mainly by merging of oligomers ($n_c \leq 5$). The shapes of the clusters are similar to the ones grown by CCA, with the exception of that now particles can be deposited straight onto a growing island. The dimension $\mathcal{D} \approx 1.5$ is higher than in ordinary CCA, as now particles can be deposited straight onto an existing cluster or in the fjords of an existing cluster.

For low F/D in Fig. 3.6 for high densities the growth is not precisely DLA-like, as clusters manage to merge. As F/D is low, even large clusters manage to diffuse enough to hit each other. The resulting clusters in Fig. 3.6 for $d = 0.14$ are therefore not entirely circular and $\mathcal{D}$ is lesser than in pure DLA.

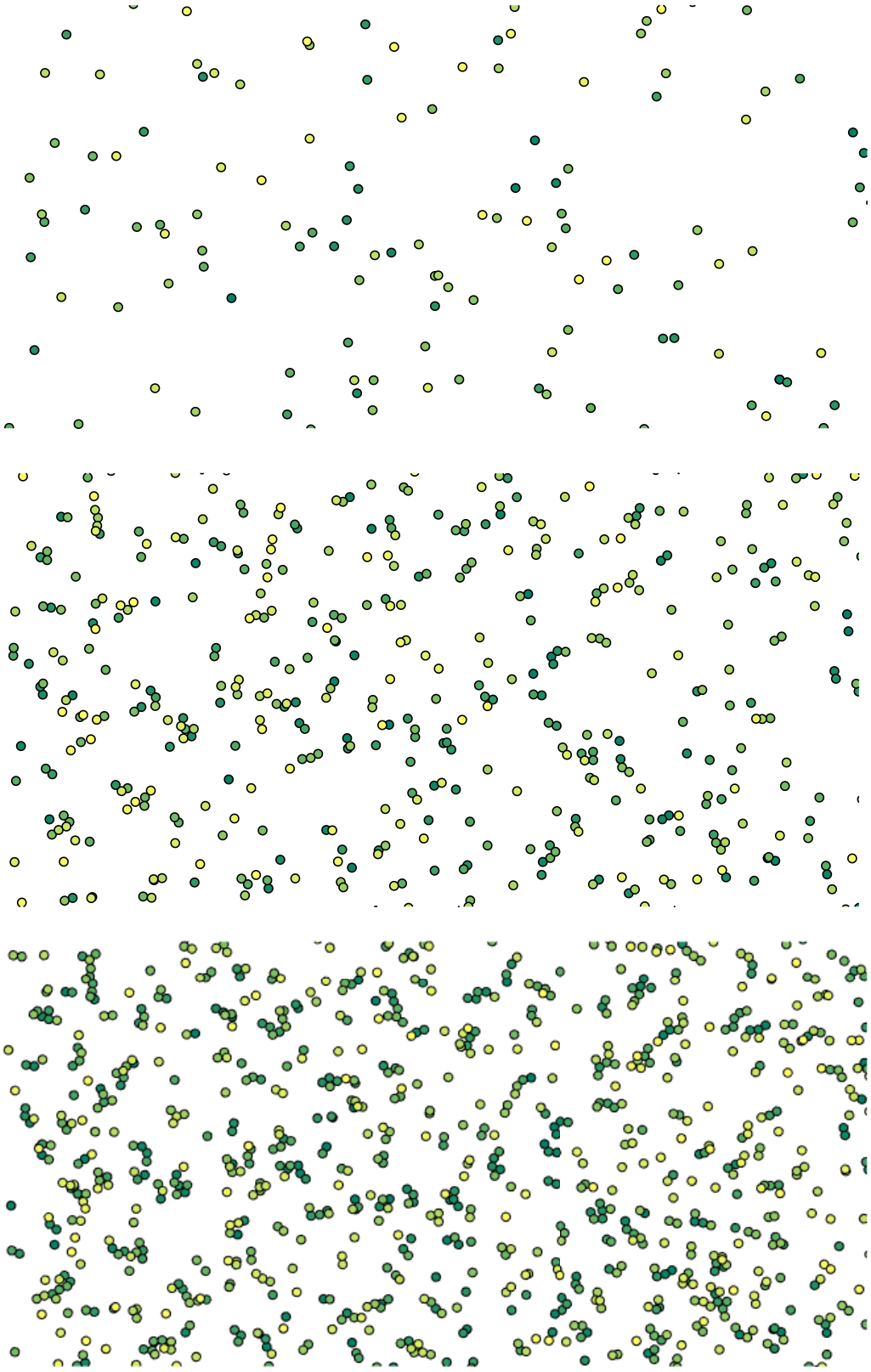

Figure 3.4: DDA in the percolation regime: clusters growing with $a = 1$, $L = 200$, $D = 0.1$ and $F = 7.85 \cdot 10^{-5}$. Growth captured for $d = 0.02$ (top), $d = 0.07$ (middle), $d = 0.14$ (bottom).

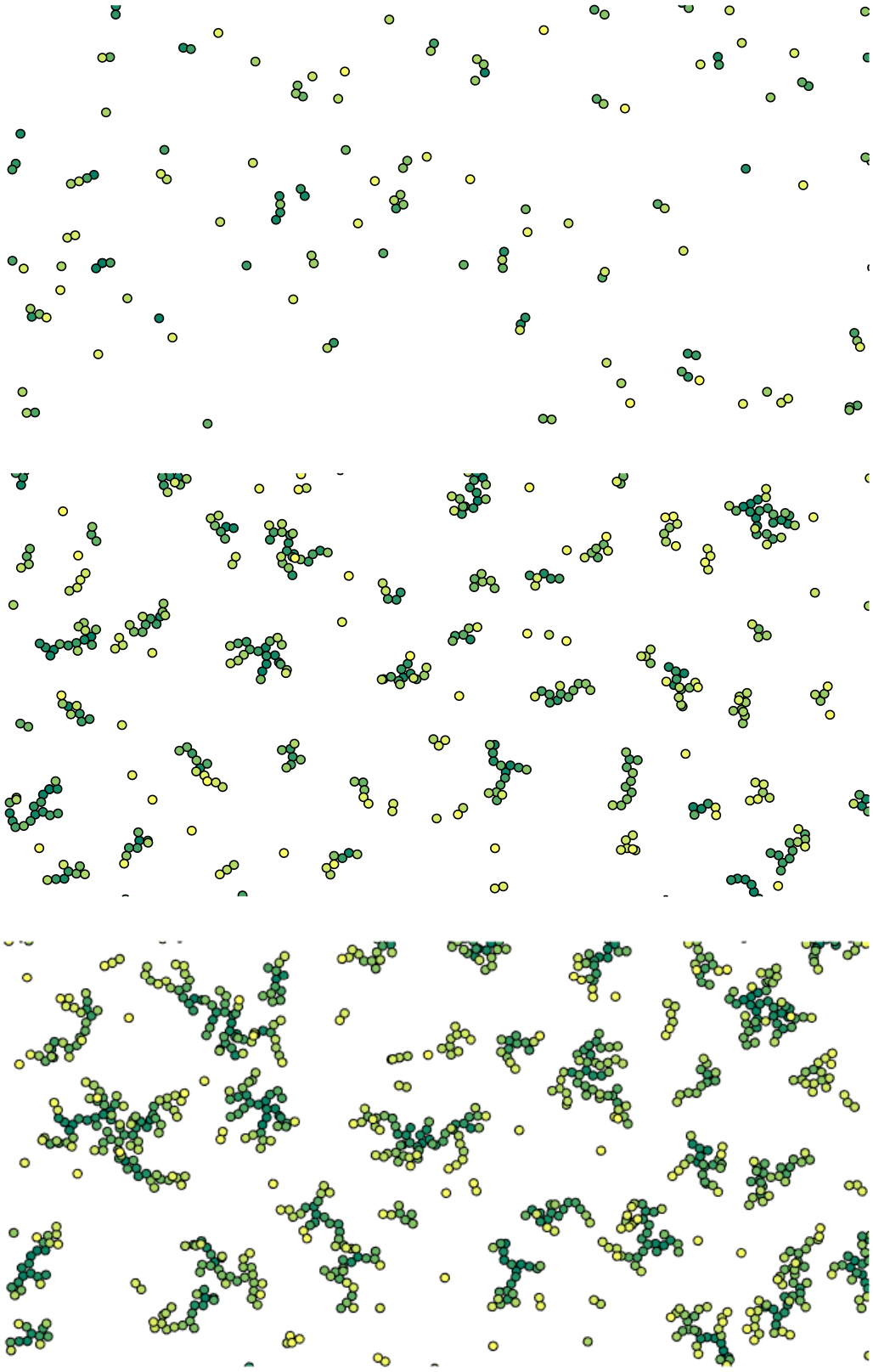

Figure 3.5: DDA in the CCA regime: clusters growing with $a = 1$, $L = 200$, $D = 0.1$ and $F = 1.57 \cdot 10^{-6}$. Growth captured for $d = 0.02$ (top), $d = 0.07$ (middle), $d = 0.14$ (bottom).

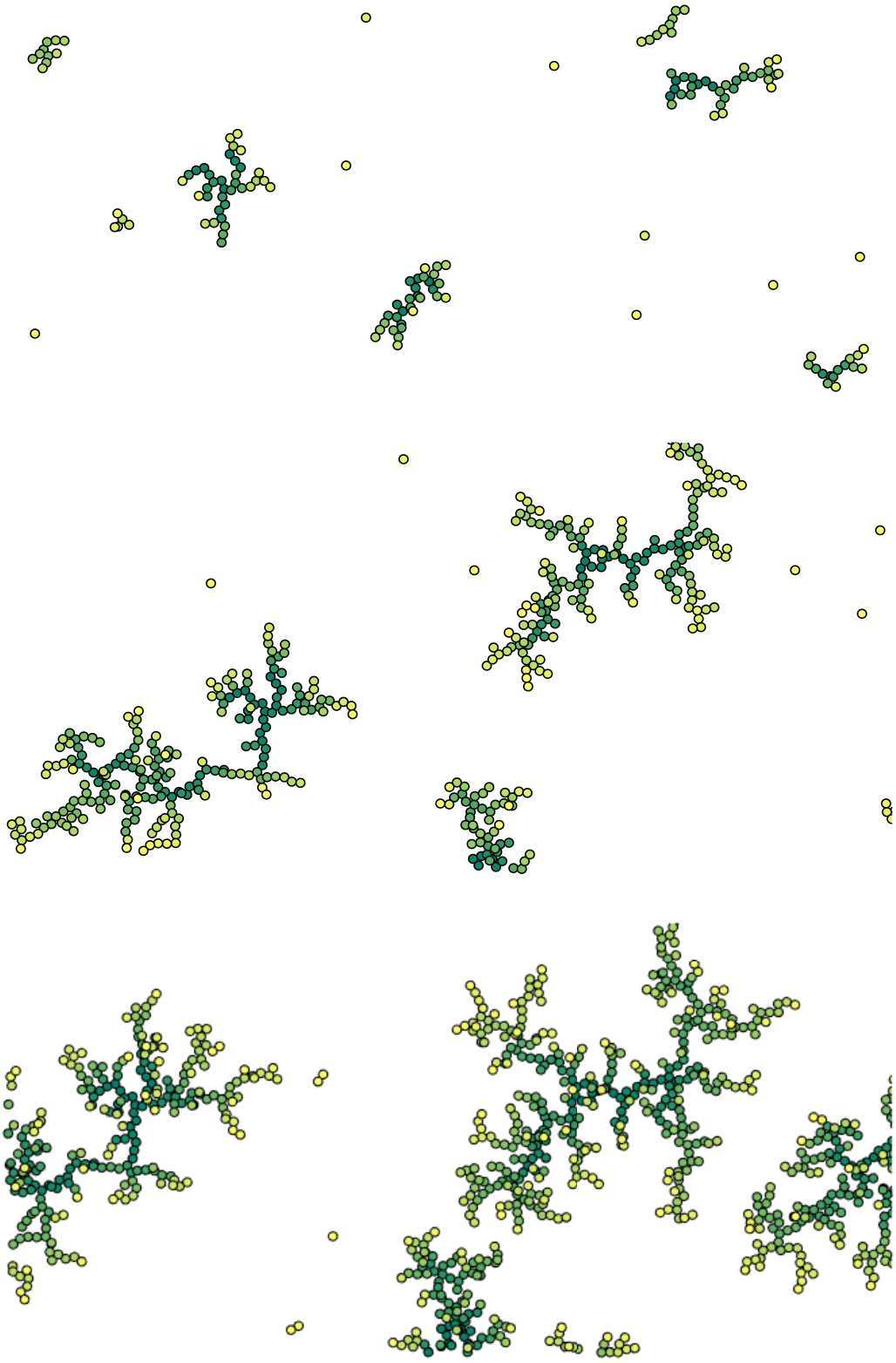

Figure 3.6: DDA in the DLA regime: clusters growing with $a = 1$, $L = 200$, $D = 0.1$ and $F = 1.57 \cdot 10^{-8}$. Growth captured for $d = 0.02$ (top), $d = 0.07$ (middle), $d = 0.14$ (bottom).

4. Modeled Experiment

The modeled experiment from Ref. [1] is growth of polymer thin films by Plasma-Assisted Vapor Phase Deposition (PAVPD). PAVPD is a method for depositing thin films from gas state. The process takes place in a vacuum chamber filled with an inert gas with pressure of about 1 Pa. The polymer precursor is put into the chamber and let to evaporate. On these vapors is then applied low-temperature plasma produced in the chamber. This turns the vapors into fragments, which are then deposited onto the substrate.

In our case the precursors were of two kinds: polyethylene (PE) and polyethylene oxide (PEO), and $\langle 100 \rangle$ Si was used as the deposition substrate. The deposition was structured in two steps as depicted in Fig. 4.1:

1. At first, PEO was deposited on the substrate long enough to cover its whole surface with a layer up to 100 nm thick.

2. Then PE was deposited onto the PEO coated surface, short enough that it did not cover it wholly.

What is special about this combination is that these two precursors are immiscible polymers, which is also true for plasma polymers made of them. Hence the PE fragments deposited had tendency to stick close to each other and form islands.

Other relevant experimental parameters are deposition speed and power of plasma dicharge used for fragmentation of PEO. PE deposition speed depends on the distance between the crucible containing the polyethylene molecules and the substrate, denoted h_{PE}. The closer the crucible was, the higher the deposition flux of the fragments entering the growing surface.

Power of the plasma P_{PEO} applied on PEO controlled its cross-link density: with higher power PEO was more fragmented and the produced plasma polymer was more cross-linked. Heavily cross-linked polymer layers are more rigid.

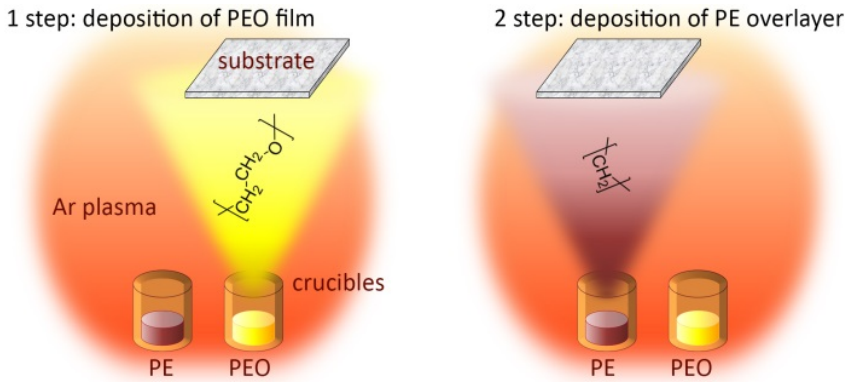

Figure 4.1: A schematic representation of the deposition procedure, image taken from Ref. [1]. At first, PEO was deposited onto the Si substrate, and then PE was deposited, forming the observed fractals.

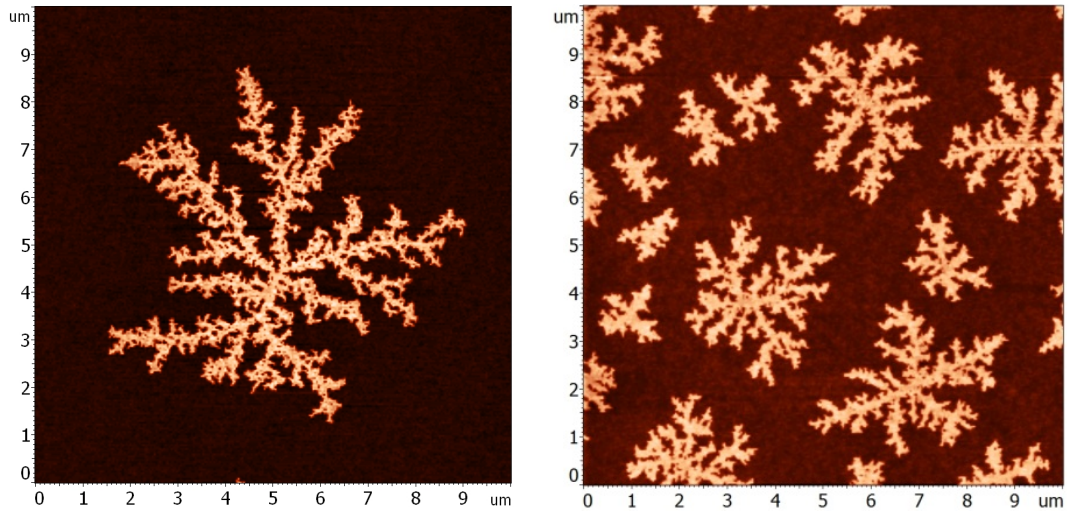

Figure 4.2: AFM images of randomly branched PE fractals grown on 100 nm thick PEO. $P_{\mathrm{PEO}} = 10$ W, $h_{\mathrm{PE}} = 20$ cm (left) and $P_{\mathrm{PEO}} = 2$ W. $h_{\mathrm{PE}} = 10$ cm (right). Branches grow and split randomly from a distinct island center.

4.1 Observed Island Morphologies

After the films were prepared, they were analyzed using Atomic Force Microscopy (AFM). It visualized the individual islands, as they were about 10 nm higher than the rest of the surface. The islands showed to have fractal shape. Fractal dimension was calculated for each of them in Ref. [1]. We have classified them into three categories:

1. *Branched fractals*, examples shown in Fig. 4.2. The islands grow from a distinct center without any preferred orientation. Island branches are random and split frequently into subbranches. They grow on less cross-linked PEO. Typical $\mathcal{D} \approx 1.62$.

2. In Fig. 4.3 are examples of *dendrites*. These grow when PEO is not present in the film or when it is very thin, as detailed in Fig.4.3 captions. They exhibit little branching from the primary branches and some degree of orientational symmetry. Typical $\mathcal{D} \approx 1.33$.

3. In Fig. 4.4 are examples of *backbone dendrites*. They are random in shape, without any preferred direction or a distinct center. The fractals are more linear, as their primary branches are more amplified. Backbone dendrites grow on highly cross-linked PEO. Typical $\mathcal{D} \approx 1.55$.

4.2 Interpretation

We now present our hypothesis of how the three distinct island types in Fig. 4.2, 4.3 and 4.4 acquired their shape. For each type, we compare it with fractals grown by one of the studied models. From this comparison we propose what physical effects were dominant in the growth of the particular island type.

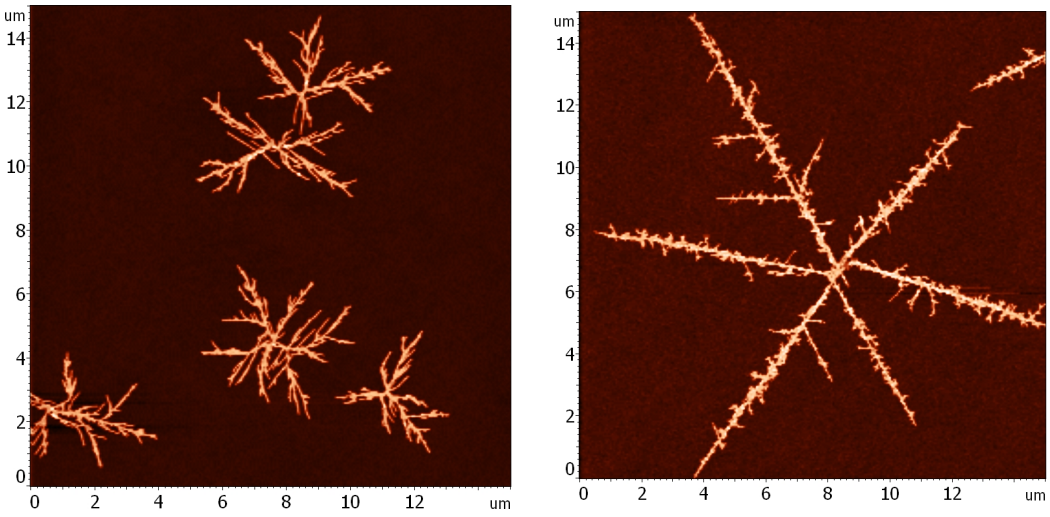

Figure 4.3: AFM images of PE dendrites grown on 15 nm thick PEO (right) and without the PEO layer (lefts). $P_{\mathrm{PEO}} = 10$ W, $h_{\mathrm{PE}} = 20$ cm. The branches of the islands grow in straight directions.

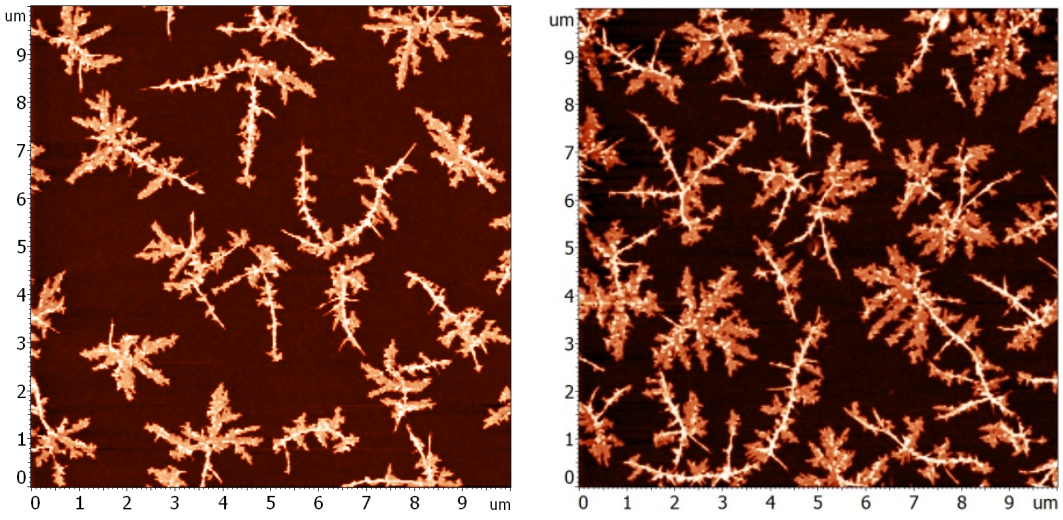

Figure 4.4: AFM images of PE backbone dendrites grown on 100 nm thick PEO. $P_{\mathrm{PEO}} = 10$ W. (left), $P_{\mathrm{PEO}} = 30$ W (right), $h_{\mathrm{PE}} = 10$ cm (both). The PEO layer was more cross-linked and deposition faster, which resulted in more linear fractals.

4.2.1 Dendrite growth

Perhaps the most surprising is the growth of the dendrites in Fig. 4.3, which closely resemble snowflakes. Snowflakes have hexagonal symmetry because the ice that forms them crystallizes in a hexagonal lattice. The deposited PE plasma polymer fragments were above their glass transition temperature (see Ref. [1]), so they were in amorphous state without any symmetry. What could then create the hexagonal symmetry of Fig. 4.3 (right)?

Results from Chap. 1 show that symmetric shapes can grow through the DLA process on a symmetric lattice. The PEO layer on which the PE diffused, however, was also above glass transition and did not have any symmetry. Therefore, the only element that could serve as the lattice was the Si substrate. That correlates with the fact that dendrites grew for thin PEO layers, where the influence of Si was stronger.

Fig. 4.5 shows the similarity between the experimental and theoretical patterns. We therefore conjecture that the attractive London forces between PE and Si are what governs the growth shape, even for a PEO layer as thick as 15 nm (Fig. 4.5) between them.

4.2.2 Growth of branched fractals and backbone dendrites

The second peculiarity is the transition from branched fractals to backbone dendrites. In Fig. 4.6 and 4.7 can be seen that one island type is similar to off-lattice DLA clusters and the second to CCA clusters. In Chap. 3 we have shown that the transition between these models happens for varying ratios of deposition flux and diffusion constant F/D.

One can shift from backbone dendrites in Fig. 4.4 to branched fractals in Fig. 4.2 in two ways: by lowering the power of plasma applied on the PEO underlayer P_{PEO} (thus decreasing its cross-link density), and/or by increasing the distance between the PE crucible and the substrate. The two branched fractals in Fig. 4.2 show this: the left one has the same P_{PEO} as Fig. 4.4 (left), but higher h_{PE}, and the right one has lesser P_{PEO} than Fig. 4.4 (left) and the same h_{PE}.

The distance h_{PE} can be simply related to F in the DDA model: with lower crucible-substrate distance h_{PE} comes faster deposition flux F, as more molecules from the crucible reach the substrate.

The physics of transition caused by the change in plasma power P_{PEO} is more subtle. It should have no effect on deposition speed F. Hence we conclude that P_{PEO} affects the diffusion coefficient of deposited PE oligomers (and clusters), $D(n_c)$, cf. Eq. (3.1).

The diffusion coefficient can change in two respects: either by changing the base diffusion coefficient of deposited oligomers D_0, and/or by changing the dependence of the cluster diffusion coefficient $D(n_c)$ on the cluster size, i.e., by altering the exponent γ.

The PEO layers with higher cross-link density are more rigid. That can affect the origin of the diffusion itself. Since the PE fragments diffuse in vacuum, the random force must come from the PEO layer or the Si substrate. More rigid PEO could, for the same temperature, have slower thermal motion. This decreases the magnitude of the random fluctuations of PEO surface and hence effectively reduces D_0.

Alternatively, it can change the scaling, as the surface now becomes more stiff and also larger clusters are able to slide on it. This would result in a decrease of γ, which would make the transition between DLA and CCA happen for lower F/D as reported in [25].

We conclude that the transition between branched fractals to backbone dendrites is the kinetic transition seen in the DDA model. It can experimentally be achieved by boosting the deposition flux or by slowing particle diffusion, for example by using more cross-linked growth surface.

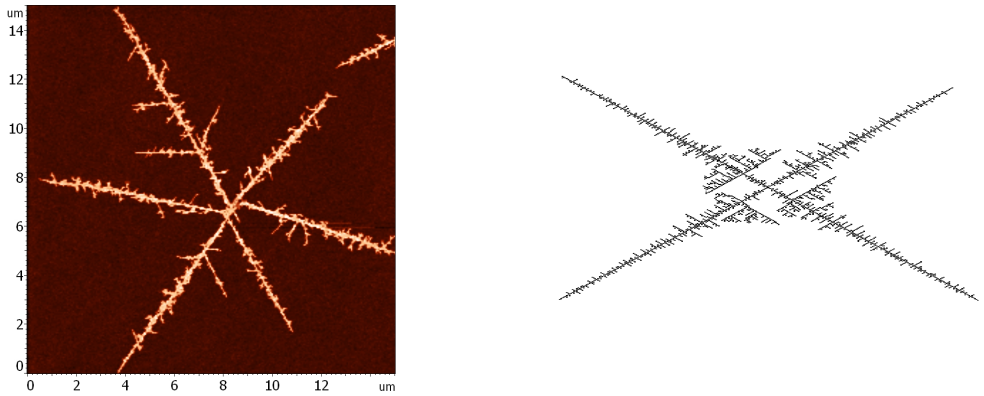

Figure 4.5: Dendrites compared to lattice DLA: A PE dendrite grown on 15 nm thick PEO compared to a square lattice DLA fractal grown with amplified diagonal preferrence ($s = 2$ on the main lattice diagonal, $s = 10$ elsewhere).

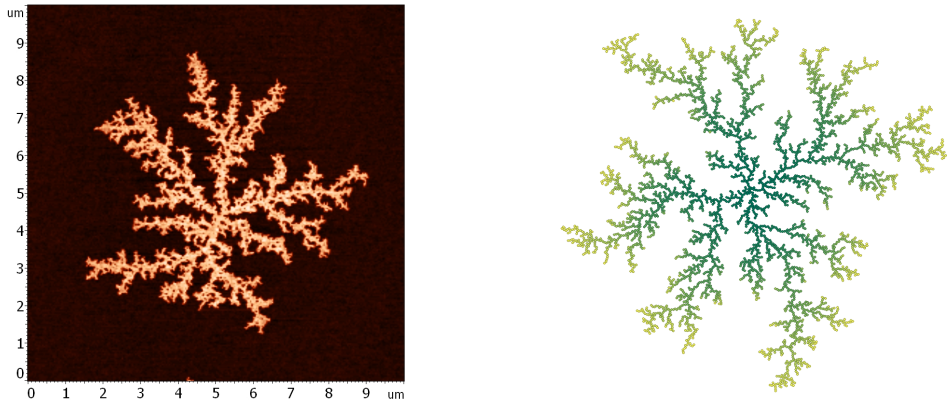

Figure 4.6: Branched fractals compared to off-lattice DLA: A randomly branched PE fractal grown on 100 nm thick PEO with $P_{\mathrm{PEO}} = 10$ W, $h_{\mathrm{PE}} = 20$ cm and an off-lattice DLA fractal.

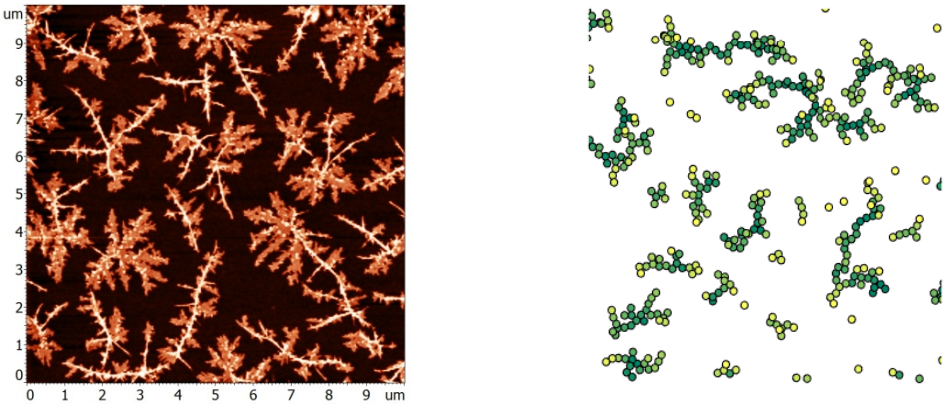

Figure 4.7: Backbone dendrites compared to the CCA model: PE backbone dendrites grown on 100 nm thick PEO, with $P_{\mathrm{PEO}} = 30$ W, $h_{\mathrm{PE}} = 10$ cm and cluster grown by DDA in the CCA phase.

Conclusion

We have developed theoretical model describing fractal growth of polymeric thin films. The modeled thin films comprise of Si substrate with a polyethylene oxide (PEO) layer, on which polyethylene (PE) was deposited. For varying experimental conditions, the PE formed fractal islands with three distinct shapes have been observed. We have reviewed existing growth models and found one that yields patterns similar to each of the shapes. The three models are lattice Diffusion-Limited Aggregation (DLA), off-lattice Diffusion-Limited Aggregation, based on diffusion of single particles, and Cluster-Cluster Aggregation (CCA), based on diffusion of clusters. Fractals grown by lattice DLA have orientational symmetry determined by the lattice. Off-lattice DLA gives randomly branched fractals with no symmetry. CCA gives linear random fractals. A more realistic model that includes deposition shows a transition between CCA and off-lattice DLA. This transition is based on competition of diffusion and deposition rates.

When the PEO layer was thin, ordered patterns similar to lattice DLA grew. This we attribute to the proximity of the Si substrate and the growing islands, where the crystalline Si acts as an effective lattice.

The other two observed PE island shapes are alike to those grown by off-lattice DLA and CCA. The transition between them was observed for varying deposition rate and varying PEO cross-link density. We therefore propose that this transition is the same as the one between DLA and CCA. This transition can be made either by speeding up deposition or altering diffusion. Cross-link density does not affect deposition, but affects diffusion, either uniformly for all diffusing clusters, or makes the larger clusters more mobile.

For more detailed information about the processes happening during the island growth, more experimental data would be needed. Namely the measurement of the crystalline properties of the PE in the nanoislands could help to determine how the deposited fragments aggregate on the surface.

Also a more realistic representation of the surface could be implemented in the simulations, as it plays a major role in both described transitions between island shapes. The cross-linked PEO could be modeled as a Gaussian Random Field, where the cross-link density could have direct effect on its correlation length. This would, however, require considerable computational power, as large two-dimensional gaussian fields are difficult to generate.

Our results clearly show that PE plasma fragments diffuse on the PEO layer even under conditions of vacuum, which is a process never reported before. We have discussed how this diffusion is influenced by the PEO layer properties, which can be fine-tuned in the experiment. In the future, this may allow for the production of highly specialized polymeric thin films.

Acknowledgement

Access to computing and storage facilities owned by parties and projects contributing to the National Grid Infrastructure MetaCentrum provided under the programme "Projects of Large Research, Development, and Innovations Infrastructures" (CESNET LM2015042), is greatly appreciated.

Bibliography

[1] A. Choukourov, P. Pleskunov, D. Nikitin, R. Tafiichuk, A. Shelemin, J. Hanuš, J. Májek, M. Unger, A. Roy, and A. Ryabov. Plasma-assisted growth of polyethylene fractal nano-islands on polyethylene oxide films: Impact of film confinement and glassy dynamics on fractal morphologies. *Submitted*, 2019.

[2] T.A. Jr Witten and L.M. Sander. Diffusion-limited aggregation, a kinetic critical phenomenon. *Physical Review Letters*, 47:1400–1403, 1981.

[3] P. Meakin. Formation of fractal clusters and networks by irreversible diffusion-limited aggregation. *Phys. Rev. Lett.*, 51:1119–1122, 1983.

[4] D.I. Bower. *An Introduction to Polymer Physics*. Cambridge University Press, 2002.

[5] Wikimedia Commons. Proposed structure for a plasma polymerized ethylene film, 2011.

[6] T. Vicsek. *Fractal Growth Phenomena*, volume 3, pages xi, 355 p. World Scientific Publishing Co, 1989.

[7] G. B. West. *Scale : the universal laws of growth, innovation, sustainability, and the pace of life in organisms, cities, economies, and companies*. Penguin Press, 2017.

[8] E. Hannezo, C.L.G.J. Scheele, M. Moad, N. Drogo, R. Heer, R.V. Sampogna, J. van Rheenen, and B.D. Simons. A unifying theory of branching morphogenesis. *Cell*, 171:242 – 255.e27, 2017.

[9] J. Theiler. Estimating fractal dimension. *J. Opt. Soc. Am. A*, 7:1055–1073, 1990.

[10] Wikimedia Commons. Fifth iteration of the cross (non-saltire) version of the Vicsek fractal, 2013.

[11] J. Nittmann and H. Stanley. Tip splitting without interfacial tension and dendritic growth patterns arising from molecular anisotropy. *Nature*, 321:663–668, 1986.

[12] T.C. Halsey. Diffusion-limited aggregation: A model for pattern formation. *Physics Today*, 53:36–41, 2000.

[13] Y. Sawada, A. Dougherty, and J.P. Gollub. Dendritic and fractal patterns in electrolytic metal deposits. *Phys. Rev. Lett.*, 56:1260–1263, 1986.

[14] J. Kertesz and T. Vicsek. Diffusion-limited aggregation and regular patterns: fluctuations versus anisotropy. *J. Phys. A: Math. Gen.*, 19:L257, 1986.

[15] P. Meakin. Structure of the active zone in diffusion-limited aggregation, cluster-cluster aggregation, and the screened-growth model. *Phys. Rev. A*, 32:453–459, 1985.

[16] D.T. Gillespie. Exact numerical simulation of the Ornstein-Uhlenbeck process and its integral. *Phys. Rev. E*, 54:2084–2091, 1996.

[17] R. Jullien, M. Kolb, and R. Botet. Aggregation by kinetic clustering of clusters in dimensions d<2. *J. Physique Lett.*, 45:211–216, 1984.

[18] H. Hentschel and J. Deutch. Flory type approximation for the fractal dimension of cluster-cluster aggregates. *Phys. Rev. A*, 29:1609–1611, 1984.

[19] R Botet and R Jullien. Intrinsic anisotropy of clusters in cluster-cluster aggregation. *J. Phys. A: Math. Gen.*, 19:L907–L912, 1986.

[20] P. Meakin. Fractal aggregates. *Advances in Colloid and Interface Science*, 28:249–331, 1987.

[21] M. Smoluchowski. Versuch einer mathematischen Theorie der Koagulationskinetik kolloider Lösungen. *Z. Phys. Chem.*, 92U.1:129–168, 1917.

[22] P.L. Krapivsky, S. Redner, and E. Ben-Naim. *A Kinetic View of Statistical Physics*. Cambridge University Press, 2010.

[23] R.M. Ziff, E.D. McGrady, and P. Meakin. On the validity of Smoluchowski's equation for cluster-cluster aggregation kinetics. *J. Chem. Phys.*, 82:5269–5274, 1985.

[24] William Mattson and Betsy M. Rice. Near-neighbor calculations using a modified cell-linked list method. *Computer Physics Communications*, 119:135 – 148, 1999.

[25] A.-L. Barabási and H.E. Stanley. *Fractal Concepts in Surface Growth*. Cambridge University Press, 1995.

[26] A. Einstein. Über die von der molekularkinetischen Theorie der Wärme geforderte Bewegung von in ruhenden FlÃijssigkeiten suspendierten Teilchen. *Ann. Phys.*, 322:549–560, 1905.

[27] K. Norregaard, R. Metzler, Ch.M. Ritter, K. Berg-Sørensen, and L.B. Oddershede. Manipulation and Motion of Organelles and Single Molecules in Living Cells. *Chem. Rev.*, 117:4342–4375, 2017.

[28] B. Cichocki and K. Hinsen. Dynamic Computer-Simulation of Concentrated Hard Sphere Suspensions - I. Simulation Technique and Mean-Square Displacement Data. *Physica A*, 166:473–491, 1990.

A. Single Particle Tracking

In this Appendix, we present an analysis of the dynamics of the diffusing particles in the CCA model based on their mean square displacement (MSD), denoted $\langle r^2(t)\rangle$.

The analysis of trajectories of diffusing particles by studying their MSD as a function of time has begin in the time of Einstein and Perrin [26]. Einstein derived that, for freely diffusing particles, the time-dependence is linear:

$$\langle r^2(t)\rangle = \mathcal{A}t. \tag{A.1}$$

For particles diffusing in complex environments such as living cells, the dependence is usually in the form of a power law [27]:

$$\langle r^2(t)\rangle \sim t^{\alpha}, \tag{A.2}$$

where for $\alpha < 1$ the process is called subdiffusive and for $\alpha > 1$ superdiffusive. Subdiffusion usually indicates that the environment has some obstacles and the particles cannot diffuse freely. Superdiffusion usually indicates that the particle's motion is actively driven by molecular motors.

In the CCA model, particles aggregate on contact. If we focus only on monomers that do not aggregate, they diffuse in an environment with many effective obstaclesobstacles formed by other particles and fractal clusters. Therefore one may expect the monomers to undergo the subdiffusion.

The averaging in MSD can be done in two ways: One can average over trajectories of many particles, or over a (long) trajectory of a single particle [27]. For N trajectories the averaging is simply:

$$\langle r^2(t)\rangle = \frac{\sum_{i=1}^{N} r_i^2(t)}{N}, \tag{A.3}$$

For averaging over a trajectory with time T, one uses:

$$\langle r^2(t)\rangle = \frac{1}{T-t}\int_0^{T-t} [r(\tau+t) - r(\tau)]^2 \mathrm{d}\tau. \tag{A.4}$$

The two approaches are equivalent for ergodic systems [27]. For the CCA model, however, they are not. The most apparent problem with (A.4) is that the environment itself is evolving. The dynamics of monomers will sure be different at the beginning, when all particles are monomers, and at the end stage, where remaining monomers avoid big clusters. Using (A.4) for small t, we merge both these processes into the value and lose information about the difference.

A.1 Results

We have performed the MSD analysis of the CCA model in the following way: The CCA model from Chap. 2 was simulated, and trajectories of all monomers were recorded. That means every τ_{MSD}-th step of trajectories of all particles was recorded, until the point where the particle aggregated ($\tau_{MSD} = 40$ for all

results below). For a CCA simulation of n particles, that produced n trajectories of varying length. The number of monomers decays quickly, so most trajectories are far shorter than average trajectory length.

Because MSD had to be calculated using (A.3), a simulation of many particles was needed. Instead of one big simulation, more simulations were run in parallel and the results were averaged. This was performed for two different densities: for $d = 0.1$ and $d = 0.25$. The results are, as shown below, quite different.

For $d = 0.1$, for large times, a typical system looked as in Fig. A.1. It consisted of myriads of CCA islands, but no island spanned the entire system from one corner to the other. The number of monomers decayed slowly, even for large times. There were many long-surviving monomers, particles that did not aggregate even on very long times.

The many-simulation averaged time-dependence of MSD is shown in Fig. A.2. For large times the behaviour has large fluctuations, as the long-survivors are still a small fraction of the original n. It shows linear behaviour, which indicates that the CCA islands are not sufficient to cause subdiffusion. For small times (Fig. A.3) tthe MSD growth is slower than linear and can be approximated by the power-law fit with exponent $\alpha = 0.92$. A typical long-surviving trajectory in Fig. A.5 explores a significant part of the system, diffusing almost freely.

For $d = 0.25$ after some time, the majority of the particles became part of one large cluster spanning the entire system: a fractal maze, depicted in Fig. A.6. Because diffusion constant scales inversely with cluster size, the maze was effectively static. The number of monomers decayed quickly and only few particles survive longer times without aggregation.

The many-simulation averaged time-dependence of MSD in Fig. A.7 has a maximum. After reaching it, MSD suddenly falls and fluctuations intensify. The dependence then becomes, on average, constant. This is because the long surviving trajectories for $d = 0.25$ look as that in Fig. A.9. The typical particle does not explore the system. It was merely initiated at a place not reached by the growing maze and stayed there for a long time. For small times (Fig. A.7 and Fig. A.8) the motion is slower than the normal diffusion and can be characterised by the exponent $\alpha = 0.78$.

For both densities, the behaviour was slower than linear for small times. To this we propose two possible explanations. One is the same as in a similar system, diffusing hard spheres [28]. For hard spheres, the environment is constant. Slower-than-linear diffusion for small times comes from short-time correlations in the particle's positions that result from other particles blocking their way.

The other possible explanation is that it is a result of the changing environment the monomers diffuse in. For small times, the system is dotted with many small obstacles and small regions of empty space. After some time, both the obstacles and the empty spaces become fewer and larger. Subdiffusion is then a result of diffusing in an emmental-like environment. The environment then turns either into a fractal maze or an archipelago of CCA clusters, and the diffusion of long-survivors copies that. Which of these two is the case can be determined by a careful analysis of time-scales in question. This represents an interesting problem for a further study.

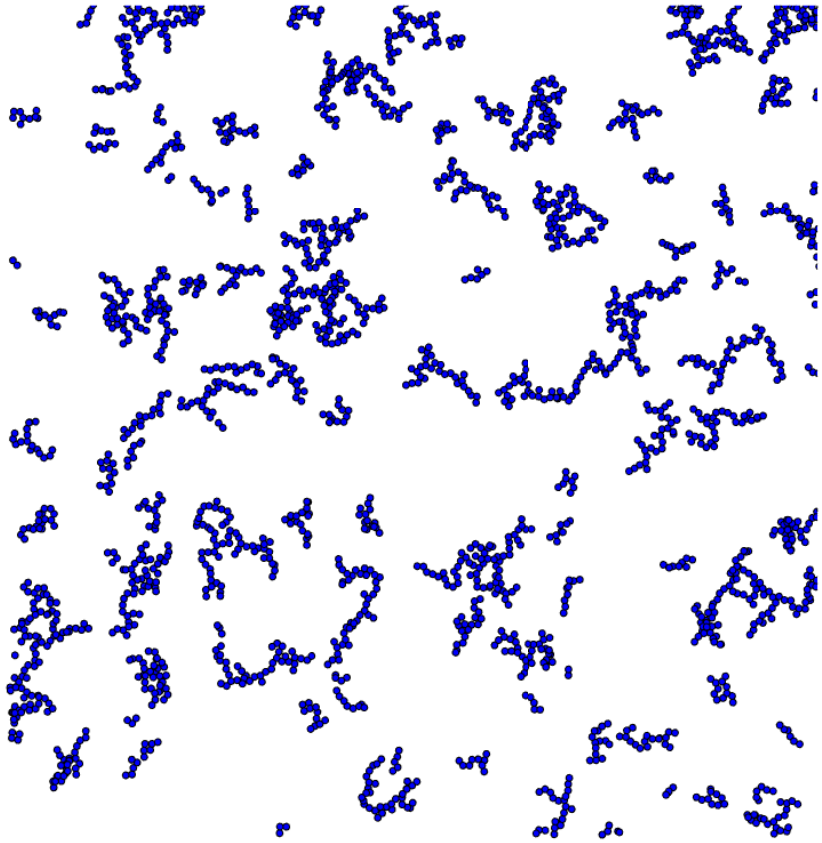

Figure A.1: A typical system grown by the CCA model for density $d = 0.1$. The particles form many large islands with free space around them. The large island move, though more slowly than the monomers.

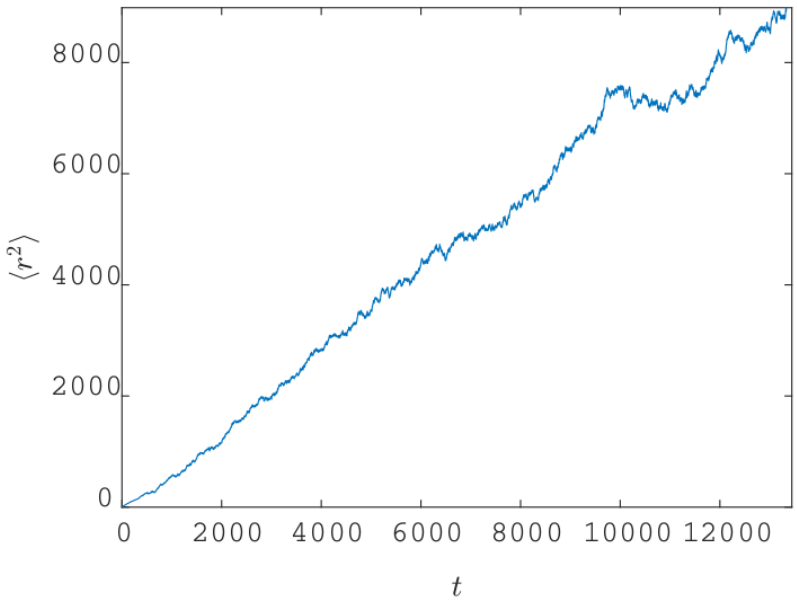

Figure A.2: Dependence of $\langle r^2 \rangle$ on t for $d = 0.1$. An average of 50 simulations of 20000 particles each. For large times, the dependence is, on average, linear.

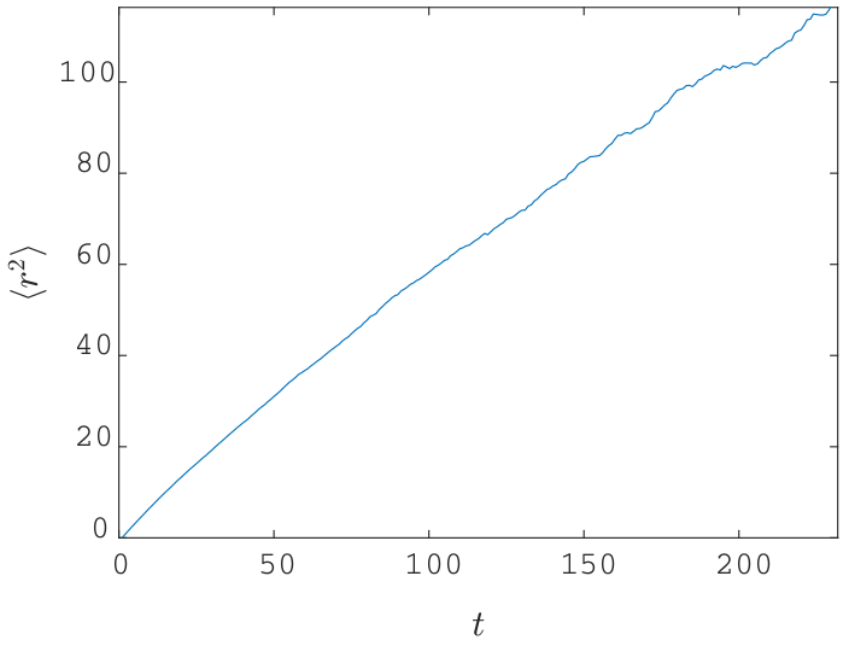

Figure A.3: Dependence of $\langle r^2 \rangle$ on t for $d = 0.1$, zoom on shorter times. An average of 50 simulations of 20000 particles each. For short times, the dependence is sublinear.

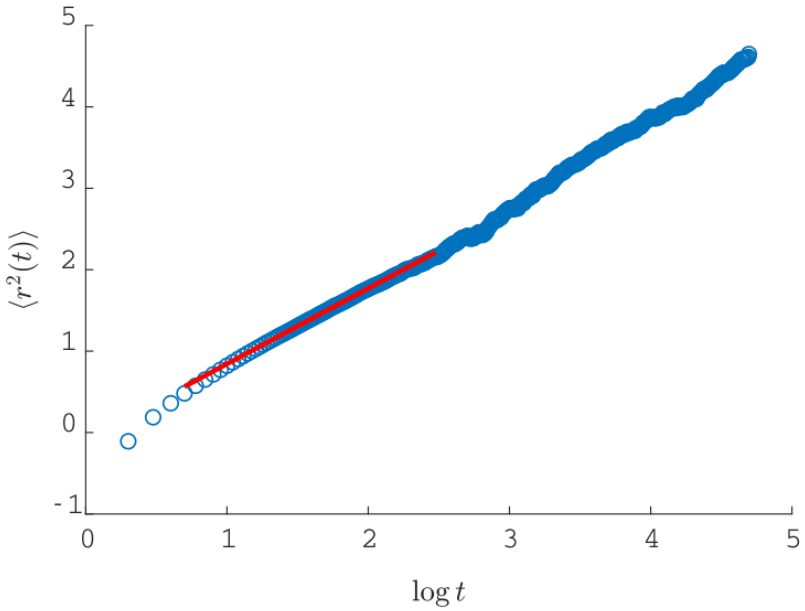

Figure A.4: Logarithmic plot of of $\langle r^2 \rangle$ on t for $d = 0.1$. An average of 50 simulations of 20000 particles each. The sublinear dependence for short times is fitted by $\langle r^2 \rangle \sim t^\alpha$ with $\alpha = 0.92$ (red line).

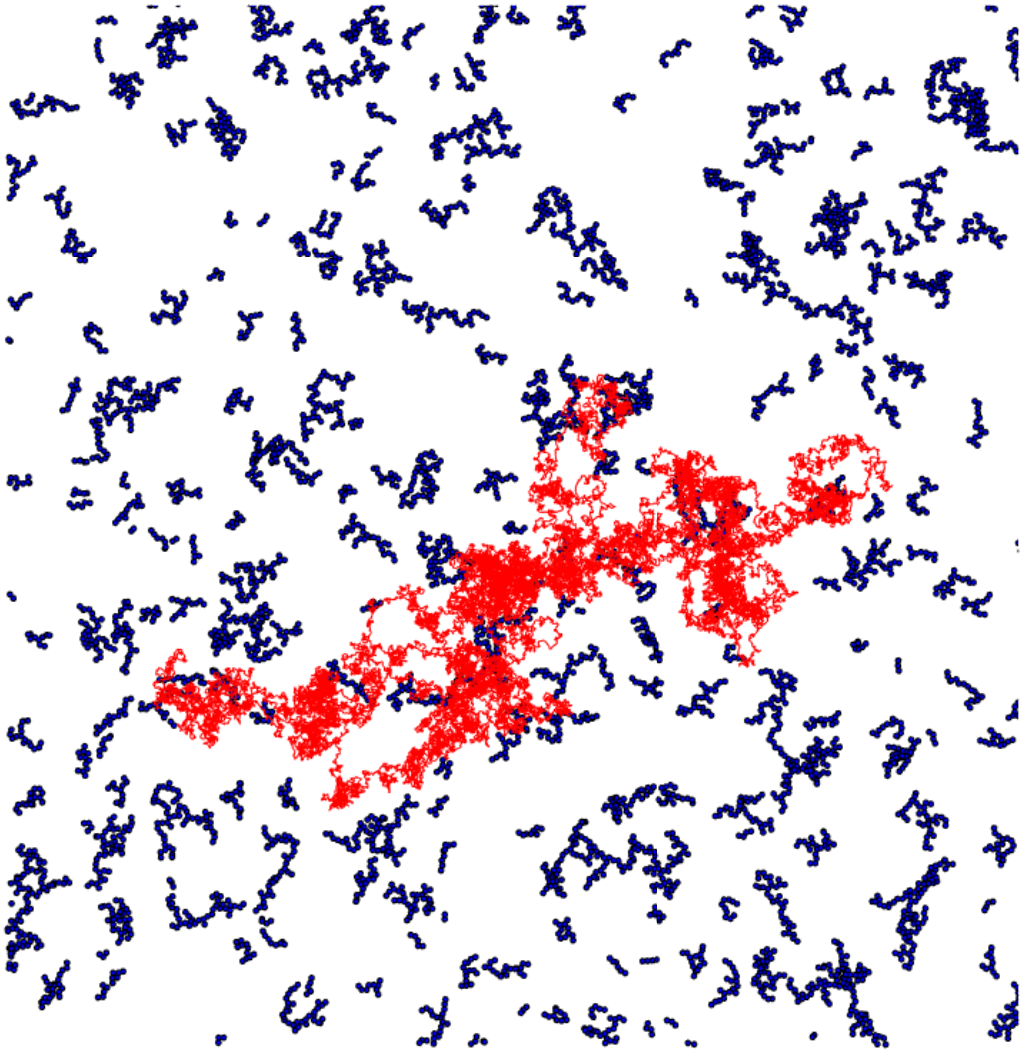

Figure A.5: Trajectory of a typical long-surviving particle for $d = 0.1$, surviving for 24000 steps. The survivor diffuses freely across the whole system. The depicted system size is $L = 200$, particle radius $a = 1$. The survivor and the other clusters move comparably fast, so the survivor's past trajectory does sometimes cross the current position of some cluster.

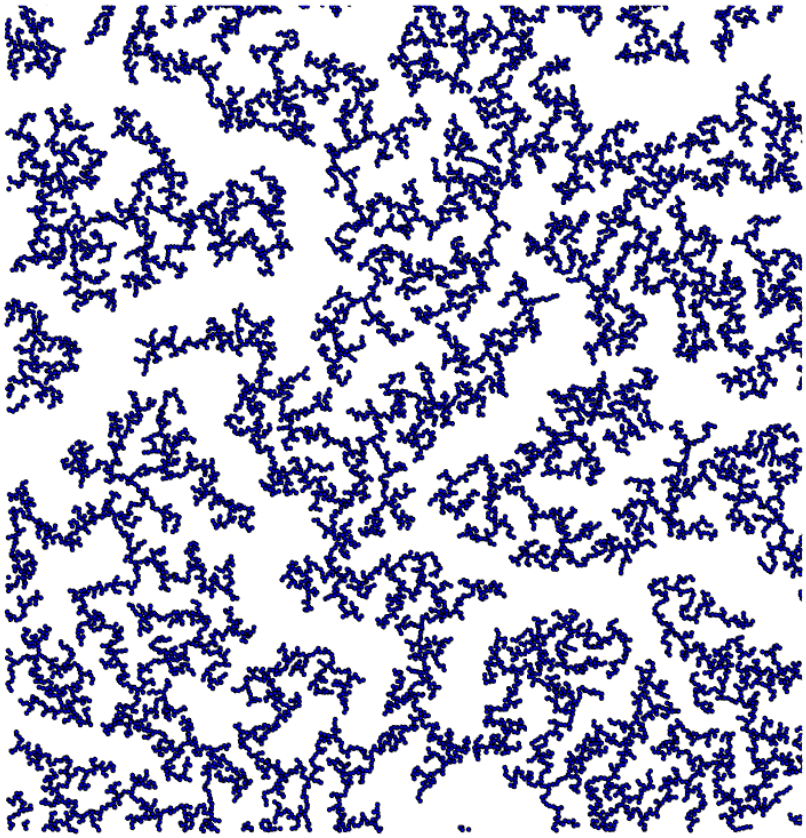

Figure A.6: A typical system grown by the CCA model for density $d = 0.25$. The particles form one large spanning cluster, which is almost static. The remaining monomers diffuse in a fractal maze.

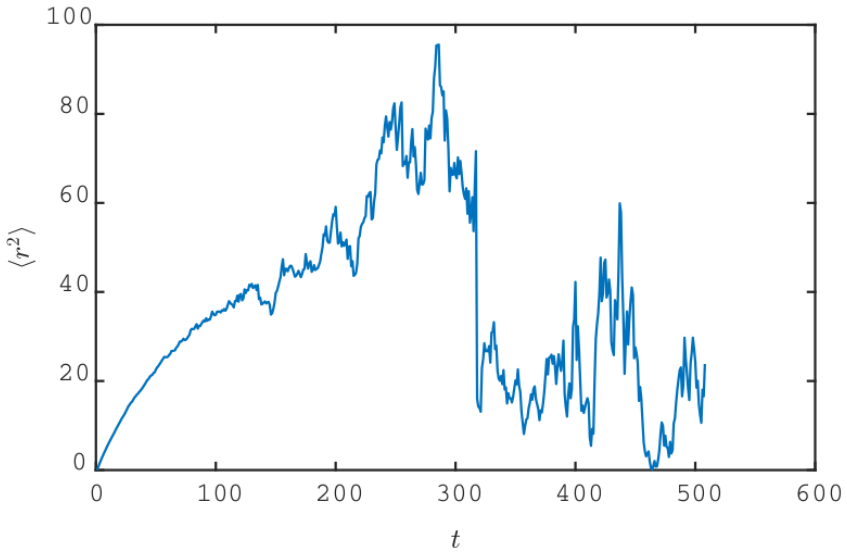

Figure A.7: Dependence of $\langle r^2 \rangle$ on t for $d = 0.1$. An average of 50 simulations of 20000 particles each. For short times the dependence is sublinear. For large times $\langle r^2 \rangle$ drops suddenly, as all particles join the spanning cluster, except the long-survivors staying almost in place.

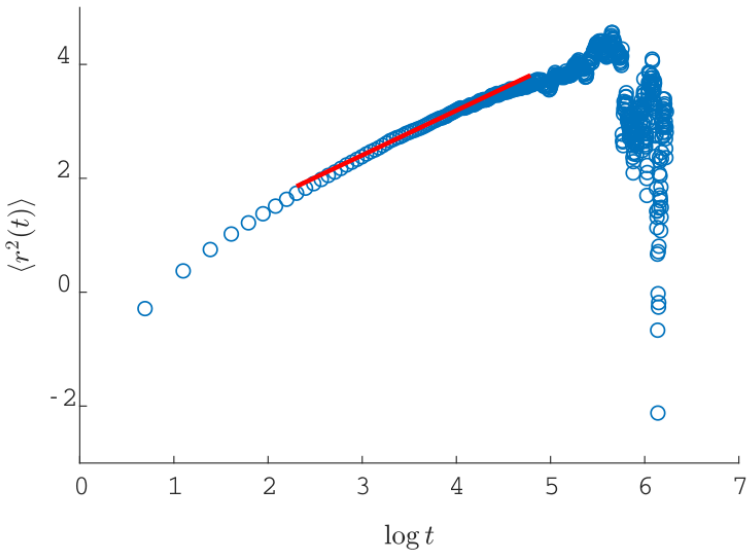

Figure A.8: Logarithmic plot of of $\langle r^2 \rangle$ on t for $d = 0.25$. An average of 50 simulations of 20000 particles each. The sublinear dependence for short times is fitted by $\langle r^2 \rangle \sim t^\alpha$ with $\alpha = 0.78$ (red line).

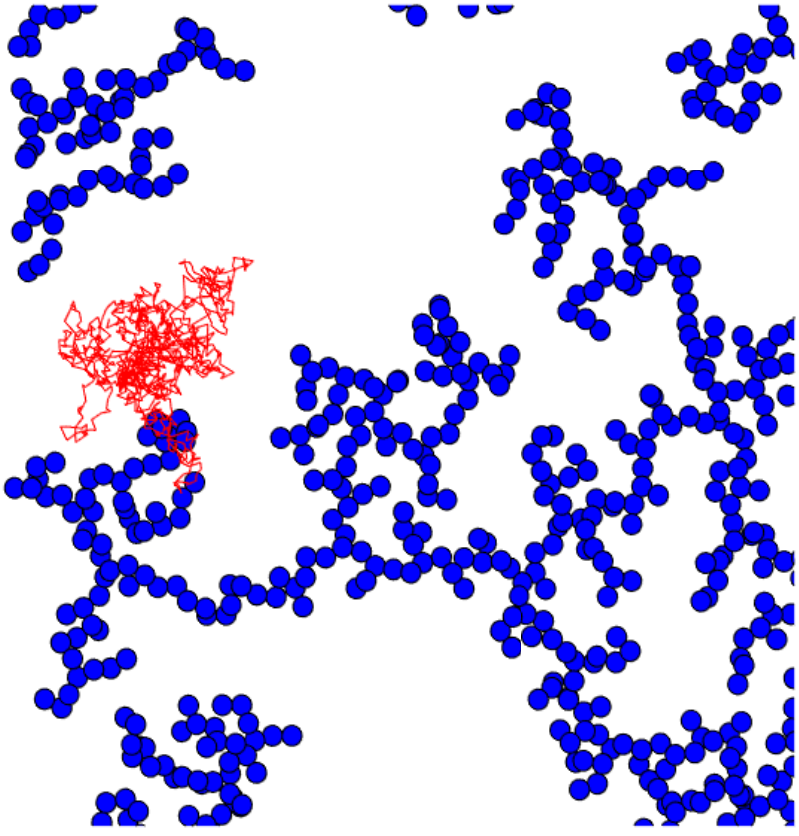

Figure A.9: Trajectory of a typical long-surviving particle for $d = 0.25$, surviving for 46000 steps. The survivor diffuses randomly in circles and stays close to its original position. It does not explore the fractal maze. The depicted system size is $L = 80$, particle radius $a = 1$.

B. Attachments

DDA simulation code

```
tic
rng('shuffle');

flag = 0;
time=0; %number of diffusion steps

%SIMULATION PARAMETERS

particleradius = 1;
diffusivity = 0.1;  %speed of diffusion
deposrate = 500; %speed of deposition
fieldsize =200; %system size (with periodic boundaries)
ninit = 1*10^1 %initial number of particles
finaldensity = 0.15; %the simulation will run until this density



% PARTICLE VARIABLES:
% surface starts with 'ninit' particles
% will simulate until density reaches 'finaldensity'
% that corresponds to 'ntotal' particles
% and 'doom' diffusion steps

n = ninint; %current number of particles on the surface
doom = (ntotal-ninit)*deposrate %simulation length

% SURFACE VARIABLES
% layergrid is used for cell listing of clusters
% when checking for aggregation

gridsize = int16(fieldsize/particleradius/2);
layergrid = zeros(gridsize+2);

%POSITIONS AND CLUSTER COUNTING

r = rand(ntotal,2)*fieldsize; % particle positions
clpointer = num2cell(1:ntotal);    % i-th cell of this
% cell array points to the particles of the i-th cluster
clnum = n; %counts the current number of clusters
clnumtime=zeros(floor(doom/deposrate),1);

%DERIVED VARIABLES
density=n*pi*particleradius^2/fieldsize^2
flux=pi*particleradius^2/fieldsize^2/deposrate

while time<doom %working cycle
  layergrid = zeros(gridsize+2);

  if mod((time+1),deposrate)==0 && flag ==0 % checks if deposition
    occurs
      clnum=clnum+1;
      clnumtime((time+1)/deposrate)=clnum;
```

```
52        n=n+1;
53    end
54    flag = 0; % becomes 1 if aggregation occured in this cycle
55    for j=1:clnum % checks if aggregation occurs
56
57     for k=1:numel(clpointer{j}) %checks if the j-th cluster should
      aggregate
58     rival = [];       %pointer of the cluster with potential merging
59     point = clpointer{j}(k); %k-th particle of the j-th cluster
60     %runs through all particles, puts each on the grid (particle
      always occupies 2x2 cells on the grid).
61     %Checks if the grid cells are occupied by another cluster.
62     %If yes, computes distances
63     %ignores the possibility, that two a particle could find two
      near
64     %clusters
65
66     gridx= int16(floor(r(point,1)/particleradius/2+1/2))+1; %
      particle's position in the cell list grid
67     gridy= int16(floor(r(point,2)/particleradius/2+1/2))+1;
68     if sum(sum(layergrid(gridy:(gridy+1),gridx:(gridx+1))))==0 %if
      neighboring cells are empty, put particle on them
69          layergrid(gridy:(gridy+1),gridx:(gridx+1)) = j;
70
71           %if neighboring cells contain only the same cluster, put
      particle on them
72     elseif sum(sum(layergrid(gridy:(gridy+1),gridx:(gridx+1))-j))==0
73          layergrid(gridy:(gridy+1),gridx:(gridx+1)) = j;
74         % else aggregate
75     else  [fn, gn, vals] = find(layergrid(gridy:(gridy+1),gridx:(
      gridx+1)));
76          rival = vals(find(vals-j,1));  %finds the cluster with
      potential merging
77          if rival
78           points = clpointer{rival};
79           %computes euclidean distance of point and all particles of
       the rival cluster
80           if min(sum((r(points,:)-r(point,:)).^2,2)'-(4*
      particleradius^2))<0
81            clpointer{j}=horzcat(clpointer{j},clpointer{rival});
82            clnum=clnum-1;
83            clpointer(rival)=[];
84            flag=1 ;  %break two loops instead of one
85            break;
86           end
87         end
88       end
89
90     end
91     if flag==1 break; end;
92    end
93
94    %DIFFUSION
95    if flag~=1 %happens only if aggregation did not
96        time=time+1; %time is incremented by one
97        displacement = diffusivity*randn(clnum,2);
98        for j=1:clnum
99          %periodic boundaries and diffusion constant scaling
```

```
100         %(diffusivity proportional to n_c^-1)
101         r(clpointer{j},:)=mod(r(clpointer{j},:)+displacement(j,:)/
      sqrt(numel(clpointer{j})),fieldsize);
102       end
103   end
104
105 end
106
107 toc
```